ACS APPLIED MATERIALS & INTERFACES

Research Article

www.acsami.org

A Facile Method to Modify the Characteristics and Corrosion Behavior of 304 Stainless Steel by Surface Nanostructuring toward Biomedical Applications

Balusamy Thangaraj,[†,‡,∥] Sankara Narayanan T. S. Nellaiappan,[*,†,§] Ravichandran Kulandaivelu,[‡] Min Ho Lee,[*,§] and Toshiyasu Nishimura[∥]

[†]CSIR-National Metallurgical Laboratory, Madras Centre, CSIR Madras Complex, Taramani, Chennai 600 113, India

[‡]Department of Analytical Chemistry, University of Madras, Maraimalai (Guindy) Campus, Chennai 600 025, India

[§]Department of Dental Biomaterials, School of Dentistry, Chonbuk National University, Jeonju 561-756, Republic of Korea

[∥]Research Center for Strategic Materials, Materials Recycling Design Group National Institute for Materials Science, Tsukuba, Ibaraki 305-0047, Japan

Supporting Information

ABSTRACT: The study addresses how surface nanostructuring of AISI 304 stainless steel (SS) by surface mechanical attrition treatment (SMAT) influences its characteristic properties and corrosion behavior in Ringer's solution. SMAT of 304 SS induced plastic deformation, enabled surface nanocrystallization, refined the grain size, transformed the austenite phase to strain induced α'-martensite phase, increased the surface roughness, induced defects/dislocations, imparted compressive residual stresses at the surface, decreased the contact angle, and increased surface energy. The change in properties of 304 SS following treatment using 5 and 8 mm ⌀ balls for 15, 30, 45, and 60 min has caused a deleterious influence on its corrosion resistance in Ringer's solution, while an improvement in corrosion behavior is observed for those treated using 2 mm ⌀ balls. The increase in surface roughness, transformation of the austenite to α'-martensite phase, a higher extent of deformation, and the presence of larger number of defects/dislocations are main factors responsible for the lower corrosion resistance observed for 304 SS treated using 5 and 8 mm ⌀ balls in Ringer's solution. In spite of having these attributes with a relatively lower extent, 304 SS treated using 2 mm ⌀ balls offered a better corrosion resistance and exhibits a better passivity. For those treated using 2 mm ⌀ balls, the ability of the nanocrystalline surface to promote passivation outweighs the deleterious influences caused by the limited amount of deformation and defects/dislocations. Based on the findings of this study, it is recommend that SMAT of 304 SS using 2 mm ⌀ balls for 15−30 min is the optimum condition to achieve the suitable surface profile, surface characteristics with better corrosion resistance.

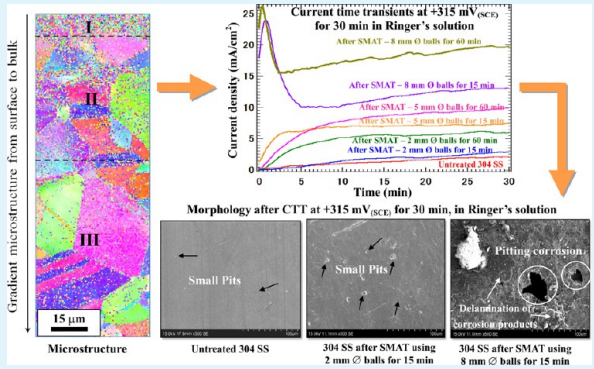

KEYWORDS: *surface nanocrystallization, plastic deformation, phase transformation, compressive residual stress, surface topography, contact angle, dislocations, corrosion behavior*

1. INTRODUCTION

Nanostructured materials have received considerable attention due to their unique physical, chemical, and mechanical properties that are explored for numerous technological applications.[1−3] Recently, nano/ultrafine grained materials produced by severe plastic deformation (SPD) have gained significant importance in biomedical applications and it could become an indispensable prerequisite for biomaterials in the near future.[4] Surface mechanical attrition treatment (SMAT) is a surface severe plastic deformation (S^2PD) method that enables the formation of a nanostructured surface layer on metallic materials and improves the overall properties and performance, without affecting their inherent properties.[5,6] Because the amount of plastic working energy incurred during treatment is relatively much less for S^2PD than for bulk deformation and most of the materials related failures originate at the surface, S^2PD assumes significance.[5−7] SMAT induces effective localized plastic deformation that results in grain refinement down to the nanometer scale. The ability to generate functionally gradient materials, with a nanocrystalline surface layer that provides the desirable surface properties and the matrix with a coarse-grained structure that offers the ductility, is a promising attribute of SMAT. Using this method, it is possible to produce thicker nanocrystalline and work-

Received: May 6, 2015
Accepted: July 21, 2015
Published: July 21, 2015

DOI: 10.1021/acsami.5b03877
ACS Appl. Mater. Interfaces 2015, 7, 17731−17747

hardened surface layers, as well as deeper surface regions with larger residual compressive stresses.[5,6] The surface nanocrystallization and refinement of grain size after SMAT helps to increase the kinetics of diffusion of boron during pack boronizing and plasma nitriding of 304 grade stainless steel (304 SS).[8,9] In addition, they also accelerate the deposition of phosphate conversion coatings on EN8-grade medium carbon steel, EN19-grade alloy steel, and H11-grade tool steel.[10]

Austenitic stainless steels are commonly used as implant materials due to their good mechanical properties, better corrosion resistance, and good biocompatibility besides the ease of fabrication at low cost. Because nano/ultrafine grained materials generated by SPD assume significance in biomedical applications, it is important to ascertain whether SMAT can be used as a surface treatment for austenitic stainless steels. SMAT alters the surface topography and increases the average surface roughness. The surface topography of materials determines its hydrophilic or hydrophobic nature. For implants, a hydrophilic surface is considered to be more desirable than a hydrophobic one in view of its better interaction with biological fluids, cells, and tissues.[11−14] In addition, generating the desired surface topography could provide significant enhancement in osteoblast adhesion, proliferation, maturation, and mineralization.[6,15,16] Nevertheless, a higher surface roughness could cause a deleterious influence on the corrosion resistance. SMAT decreases the grain size, induces compressive residual stress, microstrain, defects/dislocations, and phase transformation, all of which enable a significant improvement in hardness, fatigue resistance, and tribological properties of materials.[5,11,17,18] The correlation between grain refinement in materials produced by SPD methods and their corrosion susceptibility are still under debate, and it has been pointed out that besides the grain size, processing routes could also exert a significant influence on the corrosion resistance.[19,20] In addition, the extent of deformation, phase transformation, residual stress, microstrain, and defect/dislocation density could influence the corrosion behavior.[21,22] Bagherifard et al.[4] have shown the ability of nanocrystalline materials produced by plastic deformation to promote cell growth. According to Bahl et al.,[6] SMAT of 316L SS lead to a 50% improvement in corrosion-fatigue and enhanced the osteoblast attachment and proliferation. However, SMAT leads to a significant change in the microstructural characteristics and favors phase transformation in materials with a low stacking fault energy (SFE). The extent of change in microstructure and transformation of the austenite to the martensite phase during SMAT is a function of the type of material being treated, type and size of the balls used for treatment, frequency of vibration, and treatment time.[23,24] Because a variety of factors such as extent of surface nanocrystallization, surface roughness, extent of grain refinement, microstrain, and defect density are induced during treatment, formation of twin boundaries, volume fraction of the martensite phase, surface energy, and accumulation of internal stress could influence the corrosion resistance of stainless steels, it is important to optimize the treatment conditions so as to impart the desired properties.

In general, AISI 316 LVM stainless steel specified in ASTM F138 and F139 standards is the recommended material for stents and implant devices, particularly for those used for orthopedic surgery. AISI 304 SS is seldom used in biomedical implants and devices, except in orthodontics and implants such as archwires, brackets, and screws. Recently, Bahl et al.[6] have demonstrated the advantages of nanocrystalline surface modification of 316L SS by SMAT for the processing of metallic biomaterials used in orthopedic implants. Hence, it is clear that SMAT can be considered as a useful surface engineering method to impart the desirable characteristics needed for biomedical applications. However, among the austenitic stainless steels, the sensitivity to any signs of corrosion can be easily detected on 304 SS. In addition, the influence of transformation of austenite to martensite induced during plastic deformation by SMAT could be analyzed with the choice of 304 SS. In this perspective, the present paper aims to impart surface nanocrystallization of AISI 304 SS by surface mechanical attrition treatment (SMAT), evaluate the characteristic properties of the treated surface and to correlate the change in surface characteristics with their corrosion behavior in Ringer's solution. Because the extent of deformation and change in surface characteristics is a function of process parameters, SMAT of 304 SS is performed using 2, 5, and 8 mm ⌀ 316L SS balls for 15, 30, 45, and 60 min to determine the optimum conditions of treatment.

2. EXPERIMENTAL DETAILS

AISI 304 SS discs [dimensions, 70 mm ⌀ and 3 mm thick; composition (wt %), C, 0.04; Si, 0.57; Mn, 1.75; P, 0.019; S, 0.001; Cr, 18.10; Mo, 0.23; Ni, 8.10; Cu, 0.05; Ti, 0.003; V, 0.05; Fe, balance; average grain size, ∼ 40−50 μm] were used as substrate materials. They were buffed to a smooth finish and degreased using acetone. SMAT was performed using the surface nanocrystallization equipment (Model SNC1, Chengdu SNC Advanced Technology Co., Ltd., Chengdu, China). The schematic of the SMAT setup and the methodology have been presented previously,[21] and hence, only the salient features are provided here. The SS samples were treated using 2, 5, and 8 mm ⌀ 316L SS balls for 15, 30, 45, and 60 min. The 316L SS balls were kept at the base of the sample pot, with a load covering ∼80% of the bottom area while the 304 SS sample was fixed on the inside lid of the sample pot. The distance between the surface of the 304 SS sample and the top of the 316L SS balls was about 25 mm. The sample pot was evacuated and kept under vacuum (>5 Pa) during the entire period of treatment. The frequency of vibration was kept constant at 50 Hz.

Scanning electron microscopy (SEM; HITACHI-S3400N, Japan) was used to assess the microstructure and extent of deformation. To get a better understanding, we also analyzed the microstructural characterization of the treated 304 SS samples using electron back scattered diffraction (EBSD) measurement. For EBSD measurements, the cross sections of the treated 304 SS samples were mechanically polished using a series of SiC coated abrasive papers (200−1200 grit size) followed by 0.3 μm alumina suspension to a mirror finish. Subsequently, they were subjected to ion milling (IM 4000 Hitachi ion milling system) at an accelerating voltage of 6 kV for 30 min with a stage angle setting of 60°. The EBSD measurements were carried out on a Hitachi SU-70 SEM equipped with an EBSD system along with a TexSEM Laboratories (TSL) orientation imaging microscopy (OIM) analysis unit. The details of sample preparation, the technique and the tips and tricks were explained previously by Nowell et al.[25] Microstructural analyses were performed at several locations along the cross-section of the treated 304 SS samples, namely, at 20, 50, 100, 200, and 230 μm from the surface to the interior to verify the change in microstructure and extent of phase transformation at different depths from the surface. During analysis, the sample is tilted by 70° so as to position the electron beam within a selected grain. A selected region was considered suitable for analysis if the confidence index (CI) value was greater than 0.30, which corresponds to a 99% probability of accuracy. The Kikuchi patterns and EBSD maps were generated using the TSL-OIM analysis software.

X-ray diffraction (XRD) measurements were performed (system 3003 TT GE Technologies) using Cu Kα radiation at a step-scanning rate with a 2θ step of 0.02°/min to determine the phase contents,

DOI: 10.1021/acsami.5b03877
ACS Appl. Mater. Interfaces 2015, 7, 17731−17747

grain size, and microstrain. The average grain size of 304 SS before SMAT was determined by the intercept method using optical microscopy (Leica DMLM metallurgical microscope with QWin Image Analyzer, Germany). The average grain size of all the treated 304 SS samples were determined using the full width at half-maximum (fwhm) of the γ-Fe (111) and α'-Fe (110) planes in the XRD patterns by fitting it using a pseudo-Voigt function. The instrumental broadening was estimated using a standard silicon sample and its fwhm was subtracted from the γ-Fe (111) and α'-Fe (110) planes to calculate the actual fwhm. The broadening due to both grain size and microstrain were taken care of by considering the constituent integral breadths of pseudo-Voigt function.[26] The grain size was calculated using Scherrer's formula ($D = (0.9\lambda)/\beta_c \cos\theta$) where D, λ, θ and β_c represent the grain size, wavelength of the incident X-ray beam, diffraction angle, and integral breadth of the Cauchy component of the structurally broadened profile, respectively. The volume fraction of different phases was calculated from the integrated intensity ratios of the peaks pertaining to them.[27]

Atomic force microscopy (AFM) (AFM-Nanoscope IV, Dimension 3100 Controller, Scanning probe microscope controller, Veeco Metrology group, New York) was used to assess the change in surface topography of 304 SS after SMAT. The residual stress of treated SS samples was measured using Proto iXRD stress measurement system (Proto Manufacturing Ltd., Canada) using Cr Kα radiation. The residual stress was measured at the surface of the treated 304 SS using the $\sin^2\psi$ method by plotting the interplanar spacing of the (211) plane versus $\sin^2\psi$.[28,29] The microhardness of untreated and treated 304 SS were measured using Vickers microhardness tester (Leica VMHT (MOT), Germany) using a 50 gf load applied for 15 s. Contact angle measurements (Phoenix 300 series contact angle analyzer, Korea) were performed using double distilled water as the medium. Ten measurements were made after placing the droplet of water on sample surface for 10 s under ambient conditions and averaged out. The surface energy (E_s) was calculated from contact angle measurements.[30,31]

The corrosion behavior of untreated and treated 304 SS was evaluated by potentiodynamic polarization and electrochemical impedance spectroscopy (EIS) studies. Ringer's solution having a chemical composition (g/l) of 9 NaCl, 0.24 $CaCl_2$, 0.43 KCl, and 0.2 $NaHCO_3$ (pH, 7.40), that chemically simulates the physiological medium of the human body, was used as the electrolyte. Saturated calomel electrode (SCE) and a graphite rod were used as the reference and auxiliary electrodes, respectively. Only 1 cm^2 area of the untreated/treated 304 SS sample was exposed to the electrolyte. All the corrosion experiments were performed at 36 ± 1 °C. Potentiodynamic polarization measurements were carried out in the potential range from −250 mV_{SCE} in the cathodic direction to +1000 mV_{SCE} in the anodic direction from open circuit potential (OCP) at a scan rate of 100 mV/min. The corrosion potential (E_{corr}), corrosion current density (i_{corr}), passive current density (i_{pass}), and breakdown potential (E_b) were determined from the polarization curves. Selective samples were polarized at +315 mV_{SCE} (E_b of untreated 304 SS) for 30 min and the surface morphology of the exposed area was analyzed using SEM. EIS studies were performed at their respective OCPs. The impedance spectra were obtained using an excitation voltage of 10 mV rms (root-mean-square) in the frequency range between 10 kHz and 0.01 Hz. The EIS parameters were determined from the Nyquist and Bode plots. Before performing all electrochemical studies, the samples were allowed to remain in the electrolyte for 30 min to attain an equilibrium potential.

3. RESULTS

3.1. Effect of SMAT on Characteristics of AISI 304 SS.

The scanning electron micrographs of 304 SS after SMAT using 2 mm ⌀ balls for 60 min, 5 mm ⌀ balls for 45 min and 8 mm ⌀ balls for 60 min taken at the cross section, is shown in Figure 1. It is evident that the impingement of the 316L SS balls on the surface of 304 SS induced plastic deformation with a high strain rate during each impact. The microstructural

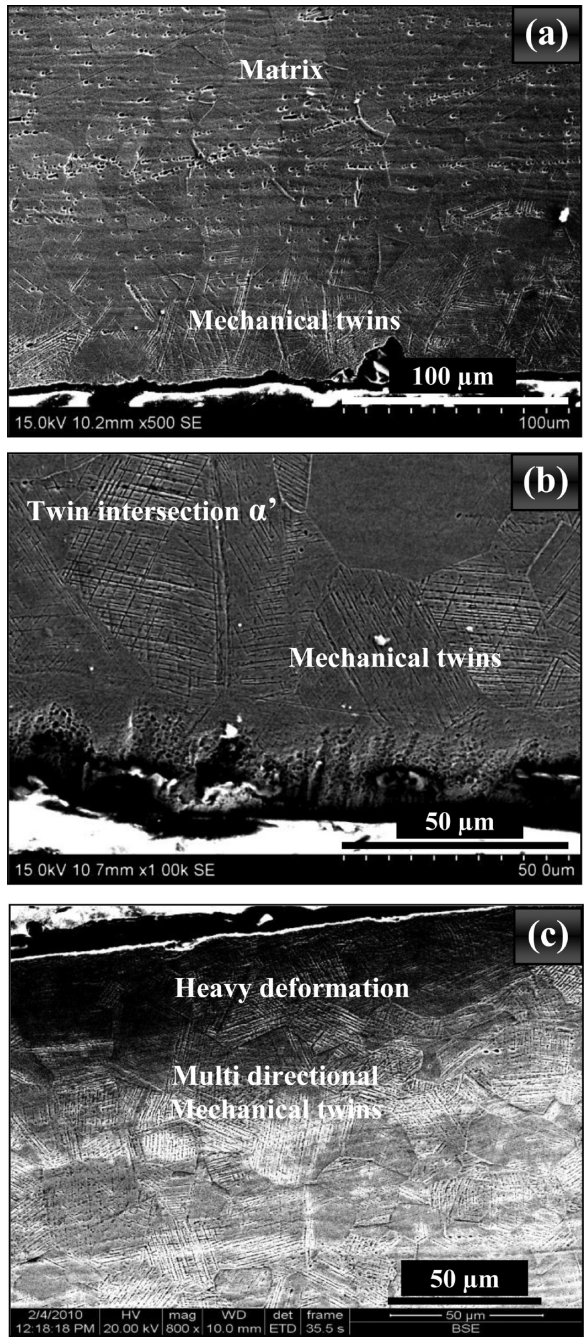

Figure 1. Scanning electron micrographs taken at the cross section of treated 304 SS showing the formation of mechanical twins and strain induced martensite during SMAT: (a) 2 mm ⌀ balls for 60 min; (b) 5 mm ⌀ balls for 45 min; and (c) 8 mm ⌀ balls for 60 min.

features reveal the formation of mechanical twins, intersection of the twins in the form of rhombic blocks and strain induced α'-martensite in the deformed region. The thickness of the deformed region and the nanocrystalline layer is largely a function of the experimental parameters such as type, number, size, and hardness of the balls used for treatment, the frequency of vibration, and treatment time. The deformation layer is much deeper for samples treated using 5 and 8 mm ⌀ balls. It is evident from the microstructural features that the heavy deformation induced during SMAT activates the twin formation that eventually becomes multidirectional. For 304

DOI: 10.1021/acsami.5b03877
ACS Appl. Mater. Interfaces 2015, 7, 17731−17747

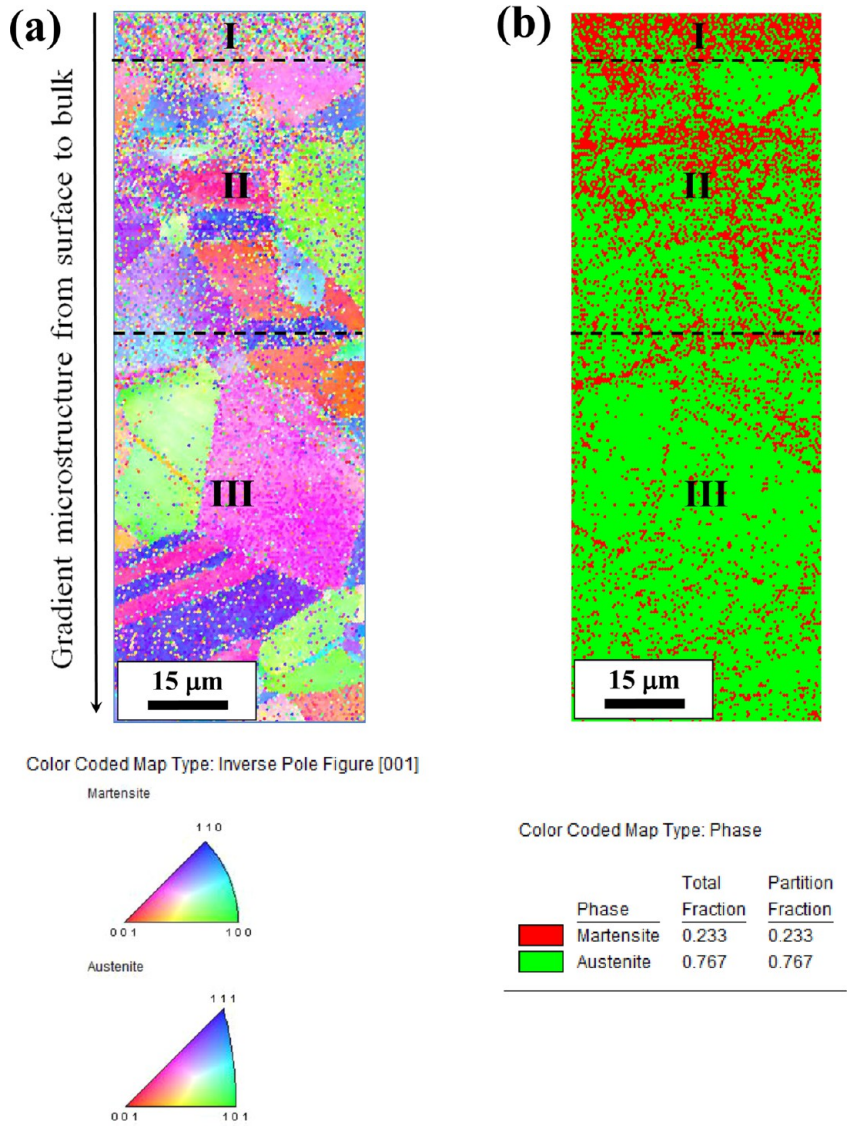

Figure 2. Grain orientation and phase distribution of 304 SS treated using 8 mm ⌀ balls for 60 min, assessed at the cross section covering a region of 130 μm from the top of the treated surface to the bulk, by EBSD analysis (top edges correspond to the top surface of the treated 304 SS): (a) inverse pole figure (IPF) map showing the orientation of fragmented and deformed grains; (b) phase contrast map taken at the same region shown in panel a, indicating the formation of the strain induced martensite phase after SMAT; red and green colors represent martensite and austenite phases, respectively; and the fraction of these phases is also included in panel b.

SS treated using 8 mm ⌀ balls for 60 min, the thickness of nanocrystalline layer is ∼30 μm.

The grain orientation and phase distribution of 304 SS treated using 8 mm ⌀ balls for 60 min, assessed at the cross section, covering a region of 130 μm from the top of the treated surface to the bulk, by EBSD analysis, is shown in Figure 2. The inverse pole figure (IPF) map (Figure 2a) shows the orientation of the fragmented and deformed grains. The phase contrast map (Figure 2b; taken at the same region as in panel a) indicates the formation of strain induced martensite phase after SMAT. The red and green colors represent the martensite and austenite phases, respectively. The variation in the microstructures (Figure 2a), as well as the volume fraction of the martensite phase (Figure 2b), of the treated 304 SS from the surface to bulk suggests a possible correlation with the extent of stain induced during SMAT. For a better understanding of this phenomenon, we also performed EBSD analysis at the cross section beginning at a distance of 50 μm from the top of the treated surface covering a region of 115 μm further down (Figure 3). The corresponding IPF and phase contrast maps are shown in Figure 3.

The X-ray diffraction patterns of untreated 304 SS and those subjected to SMAT using 2, 5, and 8 mm ⌀ balls for different periods of time are shown in Figure 4a–c. A comparison of broadening of the $\gamma(111)$ and $\alpha'(110)$ planes of untreated 304 SS and those treated using 8 mm ⌀ balls for 15 and 60 min is presented in Figure 4d. It is evident from Figure 4d that there is a considerable increase in peak broadening for 304 SS treated 8 mm ⌀ balls for 60 min when compared to those treated for 15 min. The volume fraction of α'-martensite phase formed after SMAT of 304 SS using 2, 5, and 8 mm ⌀ balls for 15, 30, 45, and 60 min is shown in Figure 5. The hardness profile of 304 SS after SMAT using 2 mm ⌀ balls for 60 min, 5 mm ⌀ balls for 45 min and, 8 mm ⌀ balls for 30 and 60 min, measured at the cross section from the surface to the bulk, is shown in Figure 6. It is evident that nanocrystallization of the surface of 304 SS

DOI: 10.1021/acsami.5b03877
ACS Appl. Mater. Interfaces 2015, 7, 17731−17747

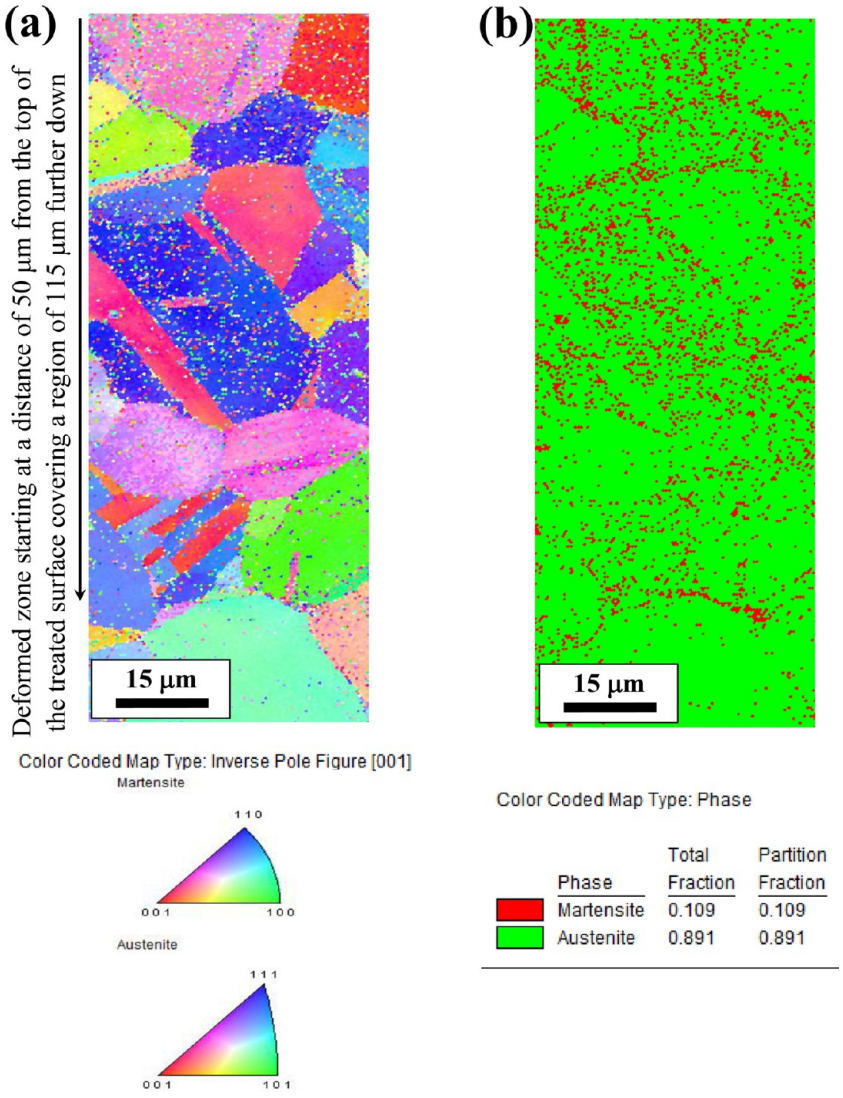

Figure 3. Grain orientation and phase distribution of 304 SS treated using 8 mm ⌀ balls for 60 min, assessed at the cross section starting at a distance of 50 μm from the top of the treated surface covering a region of 115 μm further down, by EBSD analysis: (a) inverse pole figure (IPF) map showing the orientation of the deformed grains; (b) phase contrast map taken at the same region shown in panel a, indicating the formation of strain induced martensite phase after SMAT; red and green represent martensite and austenite phases, respectively; the fraction of these phases are also included in panel b.

induced by SMAT enabled an increase in hardness from 215 (for untreated 304 SS) to 435 HV_{50gf}. The residual stress measured at the surface of 304 SS after SMAT using 2, 5, and 8 mm ⌀ balls for 15, 30, 45, and 60 min is shown in Figure 7. It is evident that there is a general trend of an increase in compressive residual stress with an increase in size of the balls and treatment time. Nevertheless, there are some exceptions to this. The compressive residual stress of 304 SS treated using 2 mm ⌀ balls for 15 min did not vary much when compared to the untreated one. In addition, the range of residual stress values is similar for 304 SS treated using 2 and 5 mm ⌀ balls for 30 and 45 min. The surface topography of untreated 304 SS as well as those treated using 2, 5, and 8 mm ⌀ balls for 60 min and, 8 mm ⌀ balls for 30 min, is shown in Figure 8. The surface roughness parameters are also included in Figure 8 for an effective comparison. It is evident that the surface of untreated 304 SS is very smooth (Figure 8a,b), while SMAT leads to an increase in the surface roughness (Figure 8c–j). For a given treatment time (60 min), an increase in size of the balls from 2 to 8 mm ⌀ leads to an increase in surface roughness (Figure 8c,e,i). To compare the effect of treatment time, we acquired surface topographic images of 304 SS treated using 8 mm ⌀ SS balls for 30 and 60 min are acquired at the same scale (Figure 8g–j). It is evident that that the surface roughness is relatively higher for the sample treated for 30 min (Figure 8g) than that of the sample treated for 60 min (Figure 8i). The change in contact angle and surface energy measured as a function of treatment time along with the shape of the water droplet formed on the surface of 304 SS treated using 2, 5, and 8 mm ⌀ balls are shown in Figure 9. It is evident that SMAT of 304 SS resulted in a decrease in contact angle (from ~79 to ~50°) and an increase in surface energy from (~13 to ~48 mJ/m^2). When compared to the untreated 304 SS, a large decrease in contact angle and a large increase in surface energy are observed for samples treated for 15 min. However, with a further increase in treatment time from 15 to 60 min, only a marginal change in contact angle and surface energy could be noticed (Figure 9).

DOI: 10.1021/acsami.5b03877
ACS Appl. Mater. Interfaces 2015, 7, 17731–17747

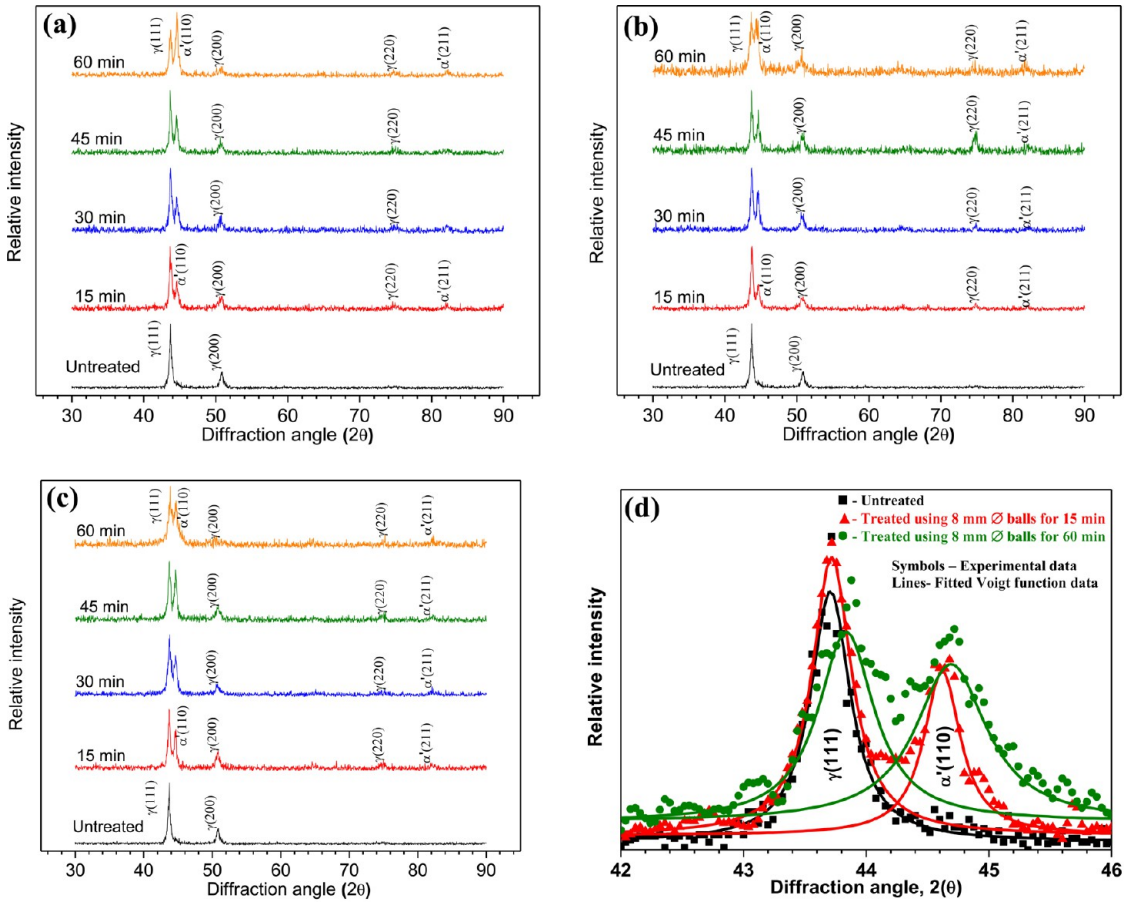

Figure 4. XRD patterns of untreated 304 SS and those subjected to SMAT using (a) 2 mm; (b) 5 mm and; (c) 8 mm ⌀ balls for 15, 30, 45, and 60 min; (d) comparison of broadening of the $\gamma(111)$ and $\alpha'(110)$ planes of untreated 304 SS and those treated using 8 mm ⌀ balls for 15 and 60 min.

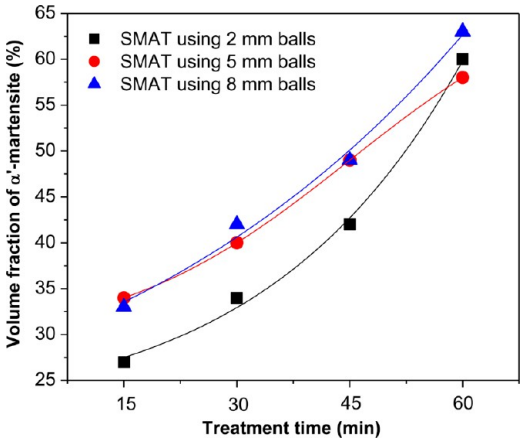

Figure 5. Volume fraction of α'-martensite phase formed after SMAT of 304 SS using 2, 5, and 8 mm ⌀ balls for 15, 30, 45, and 60 min.

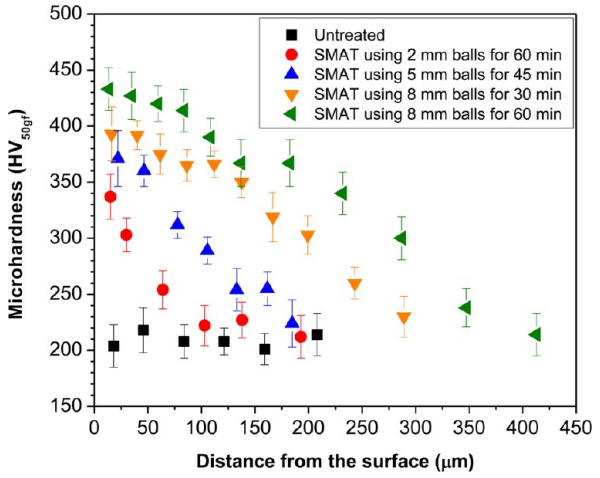

Figure 6. Hardness profiles of untreated 304 SS and those treated by SMAT using 2 mm ⌀ balls for 60 min, 5 mm ⌀ balls for 45 min and 8 mm ⌀ balls for 30 and 60 min.

3.2. Corrosion Behavior of Untreated and Treated 304 SS in Ringer's Solution.

3.2.1. Potentiodynamic Polarization Studies. The potentiodynamic polarization curves of untreated and treated 304 SS in Ringer's solution are shown in Figure 10. The corrosion potential (E_{corr}), corrosion current density (i_{corr}), breakdown potential (E_b), and average passive current density (i_{pass}), derived from the polarization curves are compiled in Table 1. When compared to the untreated 304 SS, a more positive E_{corr} and a lower i_{corr} are observed for samples treated using 2 mm ⌀ balls. However, their E_b is lower than that of the untreated one, and the extent of decrease in E_b becomes larger with an increased treatment time (Figure 10a and Table 1). For 304 SS treated using 5 mm ⌀ balls, with the exception of those treated for 15 min, the higher i_{corr} and the absence of passivation indicates an increase in their corrosion rate when compared to the untreated one. Among all the samples studied, the corrosion rate is significantly higher for those treated using 8 mm ⌀ balls, as evidenced by the more negative E_{corr}, higher

DOI: 10.1021/acsami.5b03877
ACS Appl. Mater. Interfaces 2015, 7, 17731−17747

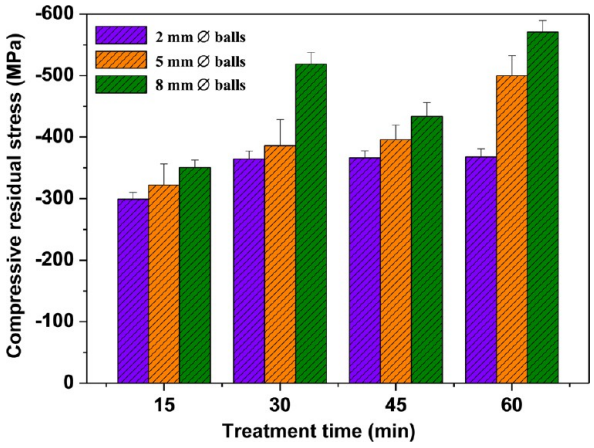

Figure 7. Comparison of the residual stress induced at the surface of 304 SS after SMAT using 2, 5, and 8 mm ⌀ for 15, 30, 45, and 60 min.

i_{corr}, and the absence of passivation. The anodic branch of the polarization curves of 304 SS treated using 8 mm ⌀ balls clearly shows the occurrence of an active dissolution (Figure 10b).

3.2.2. Current−Time Transients (CTT) Studies and Assessment of the Corroded Region. To gain better insight on the extent of corrosion protection offered by the untreated and treated 304 SS, we used current−time transients (CTT) recorded at +315 $mV_{(SCE)}$ (E_b of untreated 304 SS) for 30 min (Figure 11) and the surface morphology of the corroded region (Figure 12). The CTT clearly indicate that for a given treatment time (15 or 60 min) samples treated using 5 and 8 mm ⌀ balls exhibit a higher current density than those treated using 2 mm ⌀ balls and the untreated one (Figure 11). For a given ball diameter (2 mm or 5 mm or 8 mm ⌀), an increase in treatment time from 15 to 60 min leads to an increase in current density. The surface morphology of untreated 304 SS and those treated using 2 mm ⌀ balls for 15 and 30 min (Figure 12a−c) did not show any major signs of corrosion attack. Nevertheless, numerous small pits (marked with arrows, Figure 12a−c) could be observed on these samples. A larger corrosion pit is observed for 304 SS treated using 2 mm ⌀ balls for 60 min (marked with □, Figure 12d) when compared to Figure 12a−c along with delamination of corrosion products (marked with arrows, Figure 12d). The extent of delamination and cracking is severe on the surface of 304 SS treated using 5 and 8 mm ⌀ balls for 15 min (marked with arrow marks in Figure 12e,f). Samples treated using 5 and 8 mm ⌀ balls for 15 min also exhibit the formation of corrosion pits (marked with ○ in Figure 12e,f). The surface morphology of untreated and treated (using 8 mm ⌀ balls for 30 min) 304 SS after CTT at +315 mV_{SCE} for 30 min, along with the EDAX analysis performed at different regions, are shown in Figure 13. EDAX analysis indicates the presence of carbon, oxygen, chromium, manganese, nickel, chlorine, and iron at all regions. It is clear the amount of chlorine and oxygen are richer in the regions marked by A and C on the untreated 304 SS and in the region marked by D on the treated 304 SS. These regions also indicate the occurrence of pitting corrosion. In contrast, the amount of chlorine and oxygen is relatively less in the regions marked by B and E on the untreated and treated 304 SS, respectively.

3.2.3. Electrochemical Impedance Studies. The Nyquist plots of untreated and treated 304 SS, in Ringer's solution, recorded at their respective OCPs, are shown in Figure 14 (see Supporting Information for the Bode impedance and phase

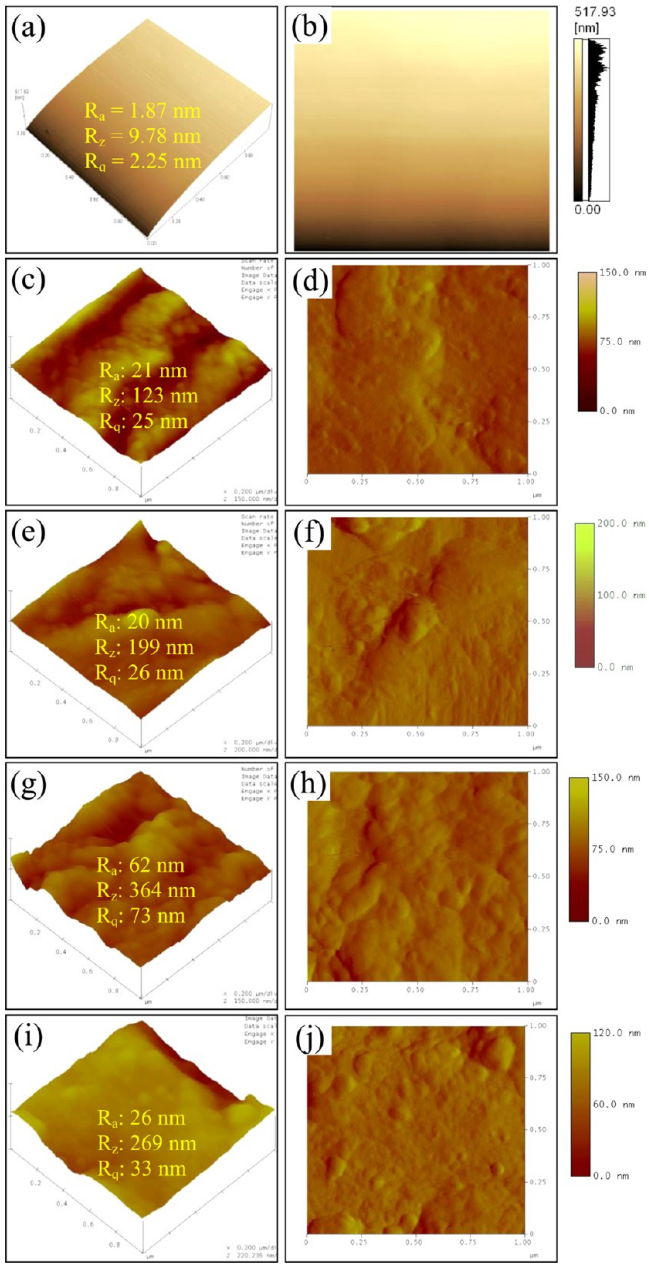

Figure 8. Surface topographic images of 304 SS before and after SMAT: (a and b) untreated; (c and d) treated using 2 mm ⌀ balls for 60 min; (e and f) treated using 5 mm ⌀ balls for 60 min; (g and h) treated using 8 mm ⌀ balls for 30 min; and (I and j) treated using 8 mm ⌀ balls for 60 min. Images were acquired at 1 × 1 μm scale.

angle plots). Different equivalent electrical circuit models are built using ZSimpWin 3.21 software and they are used to analyze the EIS data. The most suitable model is selected on the basis of best fitting (the smallest chi-square value). The proposed electrical circuit model is given in the inset of Figure 14a, and it is applicable for the analysis of corrosion behavior of untreated 304 SS and those treated using 2, 5, and 8 mm ⌀ balls for 15, 30, 45, and 60 min, in Ringer's solution. In this model, R_s represents the solution resistance. R_f and R_p correspond to the resistance of the film and polarization resistance, respectively, while CPE_f and CPE_{dl} represent the capacitance of the film and double layer, respectively. The validity of the proposed model is confirmed based on the better

DOI: 10.1021/acsami.5b03877
ACS Appl. Mater. Interfaces 2015, 7, 17731−17747

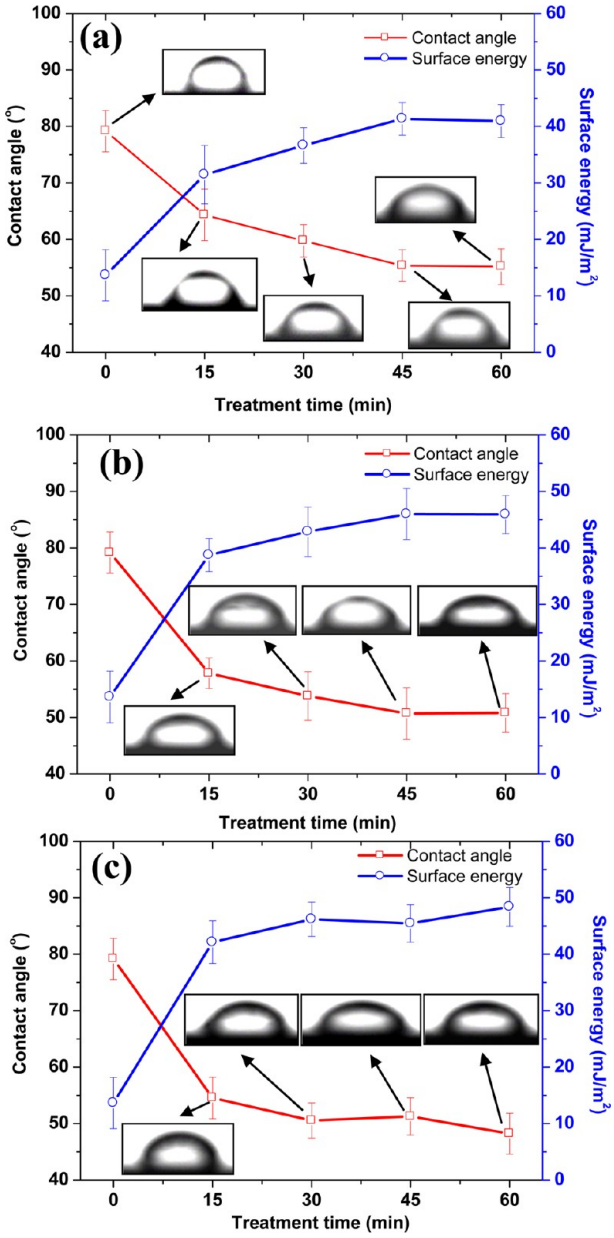

Figure 9. Variation in contact angle and surface energy along with the shape of the water droplet formed on the surface of 304 SS after SMAT using (a) 2 mm; (b) 5 mm; and (c) 8 mm ⌀ balls for 15, 30, 45, and 60 min.

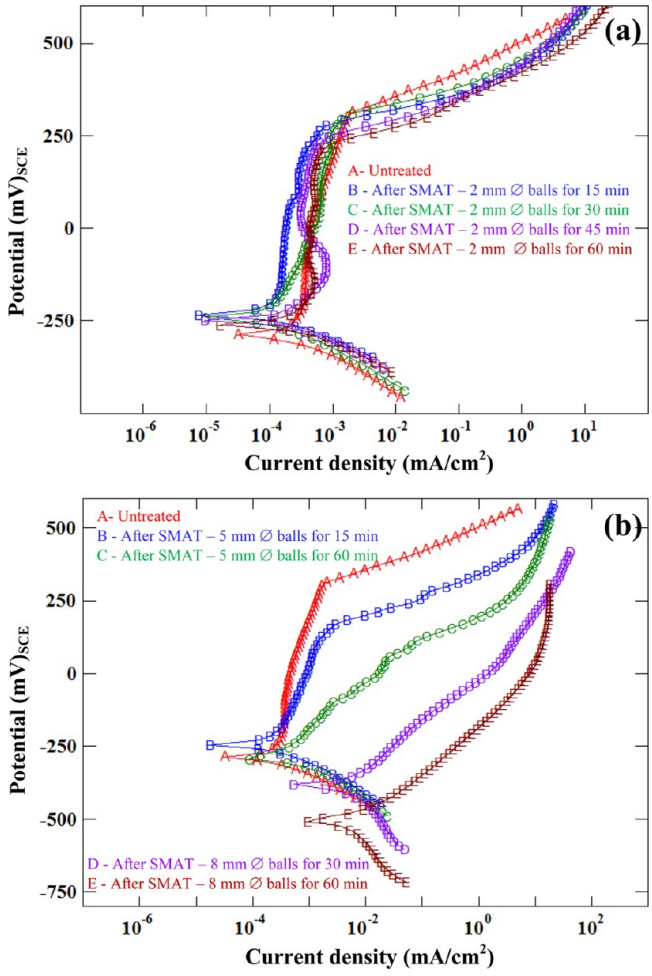

Figure 10. Potentiodynamic polarization curves of untreated and treated 304 SS: (a) untreated 304 SS and those treated using 2 mm ⌀ balls for 15, 30, 45, and 60 min; and (b) treated using 5 and 8 mm ⌀ balls for 15 and 60 min in Ringer's solution.

nonlinear least-squares fitting of the experimental data. The electrochemical parameters are derived from the EIS data after fitting them using ZSimpWin 3.21 software are compiled in Table 2. It is evident from Figure 14a and Table 2 that 304 SS treated using 2 mm ⌀ balls exhibits a higher impedance (a higher phase angle maximum over a wide range of frequencies and a higher phase angle measured at 0.01 Hz in Bode plots) than the untreated one, which signifies their ability to form a stable and compact passive film in Ringer's solution. In contrast, the lower impedance observed for samples treated using 5 and 8 mm ⌀ balls (Figure 14b,c and Table 2) imply the formation of a defective passive film on their surface that could be easily broken down by the higher concentration of chloride ions present in the Ringer's solution.

4. DISCUSSION

4.1. Characteristic Properties of 304 SS after SMAT.

The microstructures of the treated 304 SS clearly indicate that the formation of a nanostructured surface, mechanical twins, intersection of the twins in the form of rhombic blocks and strain induced α'-martensite in the deformed region (Figure 1) due to the plastic deformation induced by SMAT. It is well-known that 304 SS is a metastable austenitic stainless steel with a low stacking fault energy (16 mJ/m^2), and hence, plastic deformation by SMAT would favor the formation of a nanostructured surface layer and transformation of the austenitic to the martensite phase.[32] It is obvious to expect an increase in thickness of the deformation layer for samples treated using 5 and 8 mm ⌀ balls than those treated using 2 mm ⌀ balls due to the involvement of a higher kinetic energy when the surface of 304 SS is impinged with larger sized balls. According to Zhang et al.,[33] the mechanism of plastic deformation of 304 SS by SMAT, enabling refinement of grains and the formation of a nanostructured surface layer follows several stages: The formation of planar dislocation arrays and mechanical twins is considered the first stage. The mechanical twin formation and twin−twin interactions have much significance in the resultant microstructural features after SMAT. The 304 SS in its as-received form also show the

DOI: 10.1021/acsami.5b03877
ACS Appl. Mater. Interfaces 2015, 7, 17731−17747

Table 1. Corrosion Parameters of Untreated 304 SS and 304 SS Subjected to SMAT using 2, 5, and 8 mm ⌀ Balls for 15, 30, 45, and 60 min in Ringer's Solution Evaluated by Potentiodynamic Polarization Studies

treatment condition of 304 SS	corrosion potential, E_{corr} (mV_{SCE})	corrosion current density, i_{corr} (μ A/cm^2)	breakdown potential, E_b (mV_{SCE})	passive current density, i_{pass} (μ A/cm^2)
untreated	−288 ± 6	0.17 ± 0.03	315 ± 7	0.55 ± 0.04
2 mm ⌀ balls, 15 min	−233 ± 9	0.08 ± 0.04	278 ± 12	0.20 ± 0.05
2 mm ⌀ balls, 30 min	−240 ± 7	0.07 ± 0.02	295 ± 14	0.57 ± 0.06
2 mm ⌀ balls, 45 min	−248 ± 10	0.12 ± 0.03	246 ± 10	0.32 ± 0.04
2 mm ⌀ balls, 60 min	−261 ± 7	0.13 ± 0.04	230 ± 13	0.43 ± 0.07
5 mm ⌀ balls, 15 min	−246 ± 11	0.16 ± 0.06	184 ± 15	0.73 ± 0.05
5 mm ⌀ balls, 30 min	−259 ± 8	0.32 ± 0.05		
5 mm ⌀ balls, 45 min	−265 ± 7	0.68 ± 0.05		
5 mm ⌀ balls, 60 min	−293 ± 8	0.63 ± 0.07		
8 mm ⌀ balls, 15 min	−381 ± 10	3.60 ± 0.08		
8 mm ⌀ balls, 30 min	−436 ± 13	3.51 ± 0.12		
8 mm ⌀ balls, 45 min	−504 ± 9	5.50 ± 0.10		
8 mm ⌀ balls, 60 min	−508 ± 12	5.20 ± 0.09		

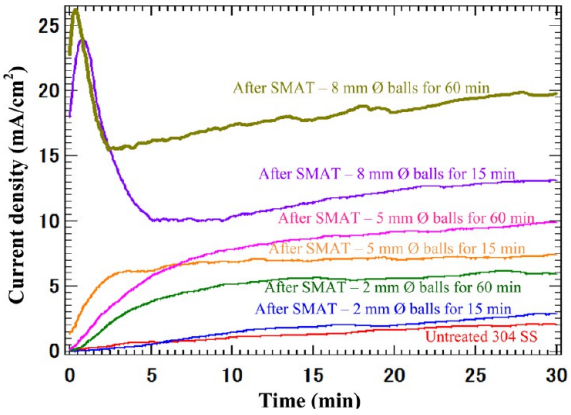

Figure 11. Current−time transients of untreated 304 SS and those subjected to SMAT using 2, 5, and 8 mm ⌀ balls for 15 and 60 min, in Ringer's solution, recorded at +315 mV_{SCE} for 30 min.

presence of twins that are formed during heat treatment, which are usually termed as annealed twins. However, twin formation is activated during SMAT; the twins are are referred to as mechanical twins, and they became multidirectional with an increase in the extent of deformation. The intersection of multidirectional twins leads to grain subdivision and martensite transformation. The twin−twin interactions are considered the precursors for the formation of strain-induced martensite and nanostructure. The presence of high-density multidirectional mechanical twins at the top of the treated surface with two and one directional mechanical twins with a further increase in depth (Figure 1c) confirms the mechanism of phase transformation. The large strain induced at the surface at a very high strain rate and the repetitive multidirectional impingement of the 316L SS balls on the surface of 304 SS has enabled the formation of a nanocrystalline surface layer.

The morphologies of the deformed microstructure of 304 SS treated using 8 mm ⌀ balls for 60 min is quite different from the top of the treated surface to the bulk (covering a region of 130 μm) (Figure 2a). Based on the variation in the microstructural features, Figure 2a can be divided into three regions. The microstructure of region III (>50 μm from the top surface) shows some deformed grains. However, it is not very much affected by SMAT. In contrast, the microstructure of region I (~10 μm from the top surface) exhibits extensive grain fragmentation with a random orientation of fine grains due to the severe plastic deformation induced by SMAT. The limited resolution of the EBSD analysis restricts the resolution of fine features of the microstructure in region I. The difficulty in resolving EBSD microstructural features of stainless steels subjected to SMAT has also been reported by other researchers.[23,34] A heavy deformation of grains is also observed in region II. The evolution of the microstructural features in regions I, II, and III confirms the formation of a gradient microstructure from the surface to the bulk after SMAT. The ability of SMAT to form a graded layer structure in a variety of materials has previously been demonstrated.[5] The variation in the microstructures of the treated 304 SS, from the surface to bulk, could be directly related to the extent of strain induced on them. During SMAT, the stain rate depends on the kinetic energy of the impinging balls, which is a function of the type, size, number and hardness of the balls used for treatment, the frequency of vibration, the distance between the surface of the material and the top of the balls as well as the characteristic properties of the material being treated (hardness, stacking fault energy, etc.).[5] For a given set of conditions, the strain will be much higher at the top surface, while it is likely to decrease gradually moving away from the surface to the bulk of the sample.[35] Hence, surface nanocrystallization is limited only to a few micrometers from the top surface. The decrease in the extent of strain induced during SMAT from the surface to the bulk also results in a decrease in the magnitude of plastic deformation, limiting the extent of decrease in the grain size. Irrespective of the differences in the microstructure observed in regions I, II and III, homogeneity could be noticed at each region.

The phase contrast map (Figure 2b) clearly reveals the evolution of the martensite phase after SMAT. The presence of both martensite (red) and austenite (green) phases in the treated 304 SS further substantiates the inferences made from XRD measurements. The higher fraction of red coloration observed for ~10 μm from the top surface suggests enrichment of the martensite phase at region I. In contrast, a higher fraction of green coloration indicates the predominance of the austenite phase at region III (>50 μm from the top surface). Region II reveals the presence of both the austenite and martensite phases, with a decrease in the ratio of martensite to austenite phase toward the bulk. The variation in the volume fraction of the martensite and austenite phases from the surface to bulk is a function of the extent of strain induced during SMAT. An

DOI: 10.1021/acsami.5b03877
ACS Appl. Mater. Interfaces 2015, 7, 17731−17747

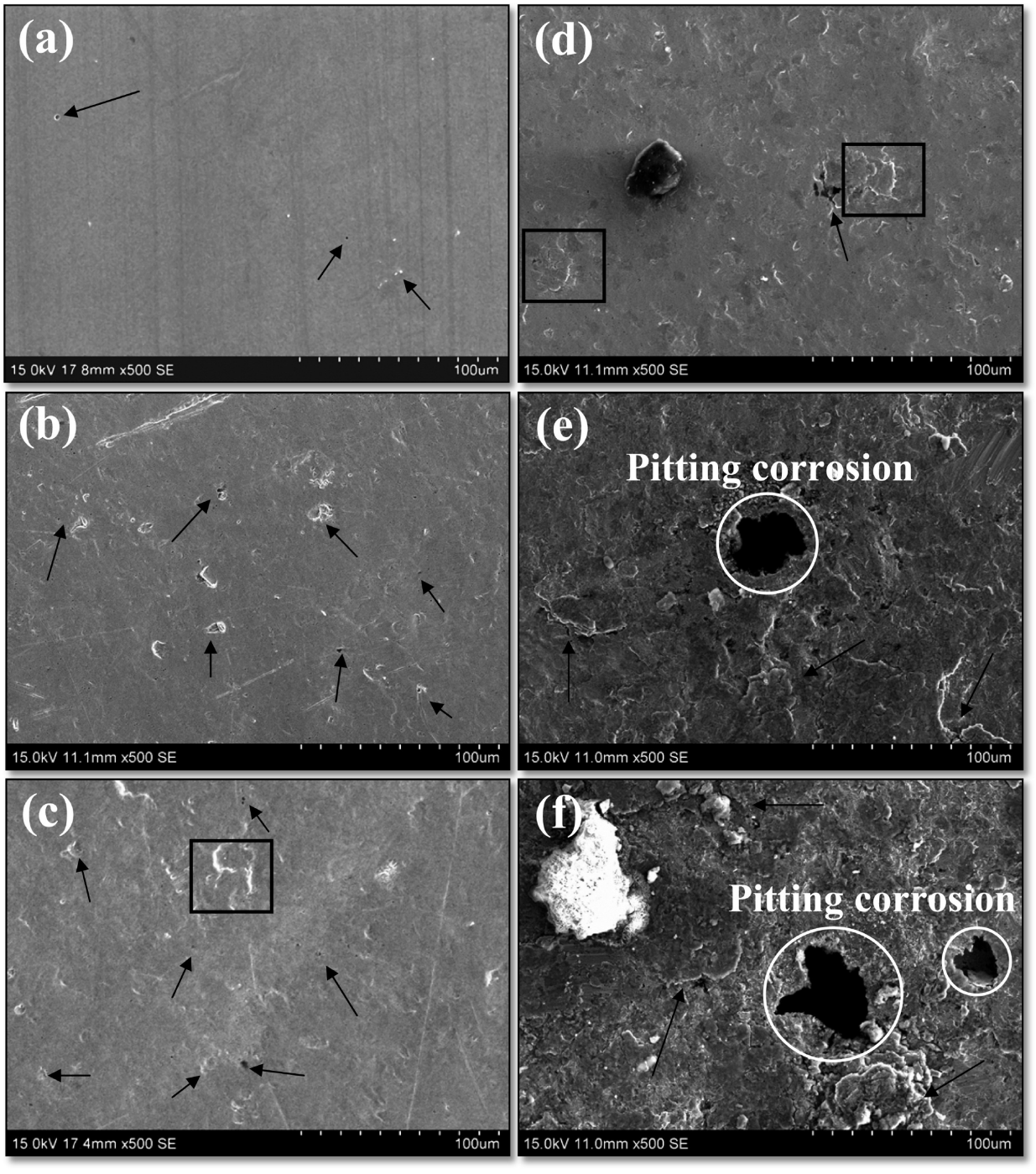

Figure 12. Surface morphology of untreated and treated 304 SS after polarizing them in Ringer's solution at +315 mV_{SCE} for 30 min: (a) untreated; (b) 2 mm ⌀ balls for 15 min; (c) 2 mm ⌀ balls for 30 min; (d) 2 mm ⌀ balls for 60 min; (e) 5 mm ⌀ balls for 15 min; and (f) 8 mm ⌀ balls for 15 min.

increase in the volume fraction of the strain induced α'-martensite phase following plastic deformation is a well-known phenomenon in 304 SS with a low SFE.[34−36] The higher strain experienced at the top surface with a gradual decrease in the strain from the surface to the bulk leads to a decrease in the magnitude of plastic deformation. The higher fractions of the martensite and austenite phases at regions I and III, respectively, and the presence of both of these phases, with a decrease in the ratio of martensite to austenite phase toward the bulk in region II, confirms that the martensite phase transformation is promoted only by the strain induced during SMAT of 304 SS.

The microstructure of 304 SS treated using 8 mm ⌀ balls for 60 min, assessed at the cross section, starting at a distance of 50 μm from the top of the treated surface covering a region of 115 μm further down (Figure 3a) by EBSD, display relatively bigger grains than those observed in Figure 2a. The corresponding phase contrast map (Figure 3b) indicates the formation of a lesser amount of martensite phase than those observed in Figure 2b. These inferences confirm the decrease in extent of stain induced during SMAT with increase in distance from the

DOI: 10.1021/acsami.5b03877
ACS Appl. Mater. Interfaces 2015, 7, 17731−17747

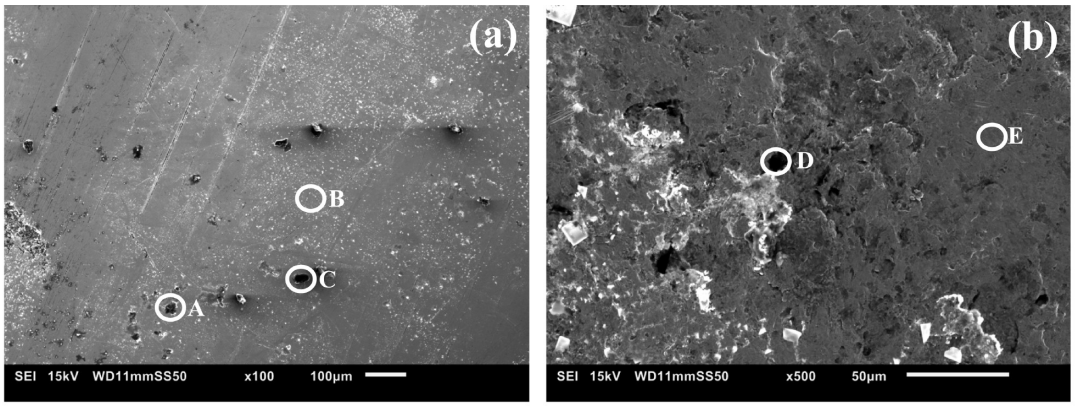

Sample	Region analyzed	Elements (wt. %)						
		C	O	Cr	Mn	Fe	Ni	Cl
Untreated 304 SS	A	17.88	7.98	15.64	1.72	49.06	4.41	3.31
	B	3.09	0.09	18.52	1.93	68.60	7.63	0.14
	C	18.43	7.34	15.97	1.79	49.01	4.41	3.05
304 SS after SMAT using 8 mm balls for 30 min	D	17.55	9.18	15.18	1.73	48.30	4.69	3.37
	E	2.70	0.71	18.86	1.84	68.40	7.48	0.01

Figure 13. Surface morphology of (a) untreated 304 SS and (b) those treated by SMAT using 8 mm ⌀ balls for 30 min after CTT at +315 mV_{SCE} for 30 min along with the EDAX analysis performed at different regions.

surface to the bulk. The fraction of the martensite phases is found to be 23% for a region covering a distance of 130 μm from the top of the treated surface to the bulk (Figure 2b) and 11% for a region covering a distance of 115 μm from a distance of 50 μm from the top of the treated surface (Figure 3b). The large difference in the volume fraction of the martensite phase estimated from XRD and EBSD analysis could be due to the limited resolution of SEM in EBSD measurement, which could have failed to identify some of the fine martensite particles.[36]

The X-ray diffraction pattern of untreated 304 SS reveals the presence of only the austenite (γ-fcc) phase. The emergence of (110) and (211) planes and the presence of both austenite and martensite (α' bcc) phases in the treated samples suggest that the transformation of austenitic to martensite has occurred only during the treatment (Figure 4). The broadening of the diffraction peaks of treated 304 SS could be attributed to grain refinement, an increase in the atomic level lattice strain induced during treatment, or both. Samples of 304 SS treated with 2, 5, and 8 mm ⌀ balls for 60 min show a considerable increase in broadening due the higher thickness of the nanocrystalline layer. When the treatment time is limited to 15 min, the thickness of the nanostructured layer will be lower, which makes the peak broadening less evident due to the concealing effect of the coarse-grained part. The average grain size of the austenite and martensite phases of treated 304 SS calculated from XRD line broadening measurements ranges from 11 to 25 nm, which is in good agreement with those reported in literature.[33] The volume fraction of the α'-martensite phase exhibits an exponential growth with treatment time rather than the size of the balls used for treatment. It appears that there is a strong dependence on the extent of deformation, which is mostly a function of treatment time rather than the size of the balls (Figure 5).

It is obvious to expect an increase in hardness following surface nanostructuring by SMAT and other researchers have also made a similar inference.[17,24] Roland et al.[17] have reported that SMAT of 316L SS using 2 and 3 mm ⌀ spherical shots for 15 min led to a hardness of 4.5 GPa at the extreme surface and, the change in hardness with the grain size follows the Hall–Petch relationship. Recently, Tsai et al.[24] reported that SMAT of 304 SS using 1, 2, and 3 mm ⌀ SUJ2 bearing steel balls (62 HRC with a smooth surface finish) has enabled a hardness of 6 GPa at the surface. According to them, in spite of the basic dependence, the trend in hardness does not follow the Hall–Petch relationship. The observed deviation suggests that besides grain size, work hardening by dislocations, and twins could have also contributed appreciably to the hardness. In the present study, in spite of a similar trend in the hardness profile (Figure 6), the hardness is slightly lower when compared to those reported in the literature.[17,24] This could be partly be due to the lower hardness of the balls (15–20 HRC) used for treatment. In the present study, the hardness measurement is performed using a microhardness tester at a distance of ~20 μm from the top of the treated surface in which the indentation marks (above 10 μm diagonal length) are very high when compared to those measured using nano indentation. Hence, the observed hardness is expected to be the combined influence of ultrafine grains and submicron grains depending on the gradient microstructure. Because the nanostructured layer is observed within a range of a few micrometers, the dislocations and twin densities could have also contributed to the measured hardness. Hence, the observed hardness is due to combined influence of the nanocrystalline surface layer, strain hardening, formation of strain induced α'-martensite and work hardening by dislocations and density of twins[17,24,37,38]

In general, the compressive residual stress is likely to increase with an increase in size of the balls and treatment time. Anand Kumar et al.[38] have also observed an increase in compressive residual stress of 718 alloy with an increase in treatment time following SMAT using 5 mm ⌀ SAE 52100 steel balls for 15–60 min. The lack of change in compressive residual stress of 304 SS treated using 2 mm ⌀ balls for 15 min when compared to the untreated one, and the similarity in the range of residual stress values observed for 304 SS treated using 2 and 5 mm ⌀

DOI: 10.1021/acsami.5b03877
ACS Appl. Mater. Interfaces 2015, 7, 17731–17747

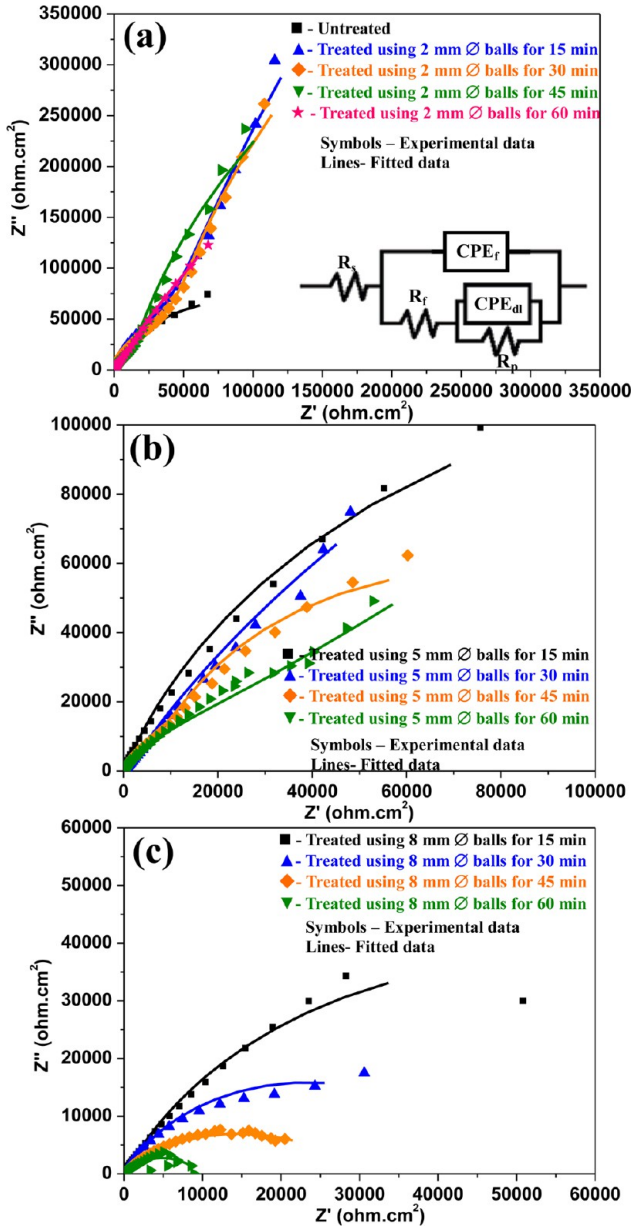

Figure 14. Nonlinear least-squares fitting obtained for the Nyquist plots of untreated 304 SS and those treated using (a) 2 mm ⌀ balls, (b) 5 mm ⌀ balls, and (c) 8 mm ⌀ balls in Ringer's solution, recorded at their respective open circuit potentials.

balls for 30 and 45 min (Figure 7) can be explained based on the distribution of residual stress during treatment. During SMAT, when the deformation proceeds into deeper layers, the residual stress is likely to redistribute through these deeper layers that result in a slight reduction in magnitude of compressive stress at the top surface layer. It has been reported that a maximum magnitude of compressive residual stress was achieved after ultrasonic impact peening of VT1−0 (α-titanium alloy) for 3 min, whereas the residual stress decreased slightly when the deformation proceeds into deeper layers.[39] Chen et al.[40] have also observed a higher compressive residual stress at the sub surface layers (50 μm below surface) when compared to the top surface after machine hammer peening.

The surface topography clearly indicates the increase in surface roughness of the treated 304 SS (Figure 8(c−j) when compared to the untreated one (Figure 8(a,b). The generation of bigger dents/dimples and an increase in the extent of deformation are considered responsible for the observed increase in surface roughness of treated 304 SS with an increase in the size of the balls from 2 to 8 mm ⌀. The relatively higher surface roughness observed for the sample treated using 8 mm ⌀ balls for 30 min (Figure 8(g,h) than those treated using similar balls for 60 min (Figures 8i,j) can be explained as follows: With an increase in treatment time from 30 to 60 min, the size of dimples is likely to decrease. When the dimples approach each other, the number of dimples per unit area would increase, resulting in increased uniformity and homogeneity of the surface. The higher working capability of 304 SS could have also permitted a decrease in surface roughness with an increase in treatment time.

The large decrease in contact angle and the large increase in surface energy observed for 304 SS samples treated for 15 min when compared to the untreated one are due to the increase in surface roughness following SMAT. Because the change in surface roughness is relatively small with an increase in treatment time from 15 to 60 min, only a marginal change in contact angle and surface energy are observed (Figure 9). Arifvianto et al.[37] have also reported about the marginal change in contact angle and surface energy with increase in treatment time during SMAT. In general, for implant applications, a hydrophilic surface is considered to be desirable than a hydrophobic one in view of its better interaction with biological fluids, cells, and tissues. The surface topographies of the treated surface confirm an increase in surface roughness of 304 SS after treatment (Figure 8). Li et al.[41] have reported that SMAT of pure Mg and Mg−1Ca alloy lead to a better wettability following an increase in surface roughness. Jamesh et al.[42] have also made a similar inference for CP-Ti subjected to SMAT. Gittens et al.[15] have reported that the introduction of nanoscale structures in combination with micro/submicro-scale roughness on Ti substrate improved osteoblast differentiation and local factor production, suggesting the potential for improved implant osseointegration in vivo. In this perspective, the increase in surface roughness, decrease in contact angle and the increase in surface energy of 304 SS after SMAT is likely to offer a beneficial influence for a better interaction with cells and tissues, thus favoring osseointegration. However, the increased surface roughness is likely to have a deleterious influence on the corrosion resistance of treated 304 SS.[27,43,44]

4.2. Corrosion Behavior of Untreated and Treated 304 SS in Ringer's Solution. The results of the potentiodynamic polarization (Figure 10 and Table 1), CTT (Figure 11) and surface morphology of the corroded region assessed at +315 mV_{SCE} (Figures 12 and 13), as well as the EIS studies (Figure 14 and Table 2), corroborate well with each other. The more positive E_{corr}, a marginal decrease in i_{corr}, similar order of current densities in CTT, and the absence of any major signs of corrosion attack observed in the morphological features and a higher impedance value signify the ability of 304 SS treated using 2 mm ⌀ balls to offer a good corrosion protection in Ringer's solution when compared to the untreated one. The more negative E_{corr}, an increase in i_{corr}, the absence of a passive region, higher current densities and general corrosion attack with a delamination of the deformed region observed in the morphological features and a lower impedance value, imply the inability of 304 SS treated using 5 and 8 mm ⌀ balls to offer a good corrosion resistance in Ringer's solution when compared to the untreated one and those treated using 2 mm ⌀ balls. The higher current density observed for samples treated using 5 and

DOI: 10.1021/acsami.5b03877
ACS Appl. Mater. Interfaces 2015, 7, 17731−17747

Table 2. Electrochemical Parameters Derived after Fitting the EIS Data for Untreated 304 SS and Those Subjected to SMAT Using 2, 5, and 8 mm ⌀ Balls for 15, 30, 45, and 60 min, in Ringer's Solution, Recorded at Their Respective Open Circuit Potentials

treatment conditions of 304 SS	R_s (Ω·cm^2)	R_f (Ω·cm^2)	CPE_f (S sn cm^{-2})	n_f	R_{ct} (Ω· cm^2)	CPE_{dl} (S sn cm^{-2})	n_{dl}	Cchi-square values ($\times 10^{-4}$)	% error
untreated	68	9.36×10^3	5.65×10^{-5}	0.80	1.71×10^5	3.01×10^{-5}	0.86	17	< 4.23
2 mm ⌀ balls, 15 min	69	1.21×10^5	1.71×10^{-5}	0.89	2.85×10^6	2.19×10^{-5}	0.96	4.2	< 2.08
2 mm ⌀ balls, 30 min	72	1.29×10^5	1.88×10^{-5}	0.86	1.41×10^6	3.04×10^{-5}	0.72	7.6	< 2.76
2 mm ⌀ balls, 45 min	70	4.90×10^4	2.24×10^{-5}	0.80	1.35×10^6	2.09×10^{-5}	0.87	8.2	< 2.87
2 mm ⌀ balls, 60 min	67	2.65×10^4	2.65×10^{-5}	0.67	1.94×10^6	3.03×10^{-5}	0.77	7.9	< 2.81
5 mm ⌀ balls, 15 min	65	4.75×10^4	1.60×10^{-5}	0.82	2.99×10^5	3.84×10^{-5}	0.80	14	< 3.85
5 mm ⌀ balls, 30 min	70	3.95×10^4	7.24×10^{-5}	0.67	5.53×10^5	1.07×10^{-5}	0.96	16	< 4.11
5 mm ⌀ balls, 45 min	71	3.99×10^4	6.13×10^{-5}	0.79	1.12×10^5	7.30×10^{-5}	0.97	12	< 3.57
5 mm ⌀ balls, 60 min	67	2.91×10^4	2.17×10^{-5}	0.73	1.59×10^5	3.71×10^{-5}	0.45	31	< 5.57
8 mm ⌀ balls, 15 min	71	6.32×10^3	1.16×10^{-4}	0.75	1.03×10^5	1.75×10^{-5}	0.83	40	< 6.40
8 mm ⌀ balls, 30 min	70	3.45×10^3	1.13×10^{-4}	0.76	3.77×10^4	1.10×10^{-5}	0.88	10	< 3.30
8 mm ⌀ balls, 45 min	69	4.69×10^3	4.14×10^{-5}	0.72	2.62×10^4	5.32×10^{-5}	0.43	8	< 2.88
8 mm ⌀ balls, 60 min	74	3.34×10^3	1.16×10^{-4}	0.59	6.37×10^3	7.42×10^{-5}	0.96	100	< 7.80

8 mm ⌀ balls, as well as those treated for 60 min, suggests a higher dissolution induced by an increase in surface roughness, increase in defect density, and the galvanic cells formed between the austenite and the martensite phases. Among the samples studied, the corrosion rate is significantly higher for 304 SS treated using 8 mm ⌀ balls. This is due to the heavy deformation induced by the impingement of 8 mm ⌀ balls that hinders the formation of a passive film and enhances the extent of corrosion attack. The severe deformation induced by SMAT, leading to the formation of many cracks and surface defects, is considered responsible for the permeation of the electrolyte, resulting in the formation of larger pits (Figure 12f). The dependence of pitting corrosion on the degree of deformation has previously been reported.[45] The presence of higher amounts of chlorine and oxygen in the regions marked A and C on the untreated 304 SS as well as in the region marked by D on the treated 304 SS along with the occurrence of pitting corrosion in these regions (Figure 13) suggests the involvement of a localized corrosion mechanism, induced by the chloride ions.

It is evident that SMAT induced plastic deformation, reduced the grain size, increased the hardness, enabled the formation of strain-induced α'-martensite phase, imparted compressive residual stress, increased the surface roughness, decreased the contact angle, and increased the surface energy. With the exception of hardness all other factors could have their own influence on the corrosion resistance of 304 SS in Ringer's solution and most importantly, their net effect on corrosion resistance is highly interdependent. Hence, establishing a direct correlation of the corrosion performance of treated 304 SS with any of these attributes is a difficult preposition. Yet, a detailed analysis is worth exploring.

Ralston et al.[19] and, Ralston and Birbilis[45] have addressed how grain size could influence the corrosion rate and passivity of various metallic alloys and how the variation in grain size could affect a specific alloy's electrochemical behavior in a specific environment. However, there is no unified theory that adequately explains the effect of grain refinement on the corrosion susceptibility of materials. By using electrochemical and atomic force microscopy studies, Pan et al.[46] have shown that deep rolled bulk nanocrystalline 304 SS and magnetron sputtered nanocrystalline 304 SS coatings offered improved passive film forming ability than conventional rolled coarse crystalline 304 SS in 0.05 M H_2SO_4 + 0.2 M NaCl. Surface nanocrystallization by shot peening using 0.8 mm ⌀ SS balls for 300 s with an average grain size of 15 nm has been shown to increase the passivation ability and corrosion resistance of 1Cr18Ni9Ti SS in 3.5% NaCl.[47] Maleki-Ghaleh et al.[48] have reported that ultrafine-grained nanocrystalline 316L SS obtained after eight passes of ECAP with a mean grain size of about 78 nm exhibits considerable improvement in corrosion resistance in Ringer's solution. In the present study, the average grain size of untreated 304 SS is about 40−50 μm, and it decreased to 11−25 nm after SMAT using 2, 5, and 8 mm ⌀ balls for 15, 30, 45, and 60 min. Under conditions that could induce passivity, nanocrystallization has been shown to promote passivation and increase the corrosion resistance.[19,45−48] Hence, surface nanocrystallization of 304 SS after SMAT is expected to promote better passivation and offer an improvement in corrosion resistance. However, the treated 304 SS displayed varying degree of corrosion resistance. 304 SS treated using 2 mm ⌀ balls showed a better tendency to form a passive film while those treated using 5 and 8 mm ⌀ balls failed to exhibit passivation. The more negative E_{corr} and a higher i_{corr} observed for 304 SS treated using 8 mm ⌀ balls when compared to the untreated one indicates a drastic decrease in corrosion resistance in spite of a considerable reduction in grain size following SMAT (Figure 10 and Table 1). Hence, it is clear that the corrosion behavior of treated 304 SS is not solely dependent on grain size. Grain refinement is considered an important attribute in metallic materials used as implants in terms of achieving improved strength, hardness, fatigue resistance, surface topography, cellular response and bioactivity.[4,15,49] Yet, a better corrosion resistance is also equally important for implants, and hence, it is important to understand how the processing route and parameters influence the corrosion behavior in order to optimize the treatment conditions. This inference further supports the views of Gupta and Birbilis,[20] who pointed out that processing route and the associated processing parameters impart significant microstructural changes, which needs to be thoroughly investigated in terms of the corrosion behavior of SS. The observed variation in corrosion behavior of 304 SS treated using 2, 5, and 8 mm ⌀ balls for 15, 30, 45, and 60 min indicates that besides grain refinement, other factors such as increase surface roughness, phase transformation (strain induced α'-marten-

DOI: 10.1021/acsami.5b03877
ACS Appl. Mater. Interfaces 2015, 7, 17731−17747

site), defects/dislocations and residual stresses induced during SMAT should also be considered while accounting for the corrosion behavior of 304 SS in Ringer's solution. Further, the solubility of corrosion products, composition and compactness of the passive film, semi conductive properties of the passive film, pH, and corrosivity of the medium should also be considered. Establishing a direct correlation of the corrosion behavior of treated 304 SS with any one of these factors is difficult and complex since it is influenced by more than one factor at a time. All these factors, either individually or in combination could influence the corrosion resistance of the treated 304 SS.

In general, an increase in surface roughness lead to a higher corrosion rate of metallic materials following the increase in their practical surface area, which serves as active sites for the electrochemical reactions.[27,43,44,50,51] In the present study, SMAT of 304 SS using 2, 5, and 8 mm ⌀ balls has resulted in an increase in surface roughness. However, those treated using 2 mm ⌀ balls enabled a more positive E_{corr} and a slightly lower i_{corr} when compared to the untreated one. In contrast, 304 SS treated using 5 and 8 mm ⌀ balls lead to a more negative E_{corr} and a higher i_{corr} when compared to the untreated one. Passivation is quite evident in 304 SS treated using 2 mm ⌀ balls, whereas the formation of a passive film is totally prevented for those treated using 5 and 8 mm ⌀ balls. If the increase in surface roughness is considered responsible for the increase in corrosion rate and lack of passivation of 304 SS treated using 5 and 8 mm ⌀ balls, then the improvement in corrosion resistance and the formation of an intact passive film on 304 SS treated using 2 mm ⌀ balls could not be explained. The lack of a direct correlation between surface roughness and corrosion rate has also been reported earlier. Shahryari et al.[50] and Lee et al.[51] and have observed a poor correlation between polarization resistance and surface roughness of 316 SS and 21Cr ferritic SS when their average surface roughness was relatively higher than 0.5 μm. In our earlier study,[21] we have observed that in spite of an increase in surface roughness of 409 SS from 0.33 μm to 0.54−0.60 μm, following SMAT using 2 mm ⌀ balls, the treated 409 SS offered a better corrosion resistance and displayed better passivation behavior when compared to the untreated counterpart. Chui et al.[43] have reported that an increase in surface roughness of 316L SS from 0.39 to 0.53 μm after fast multiple rotation rolling lead to a decrease in corrosion resistance in 3.5% NaCl. Yet, it did not totally prevent the formation of a passive film. Hence, it is clear that besides surface roughness other factors such as phase transformation (strain induced α'-martensite), defects/dislocations and residual stresses induced during SMAT should be considered while accounting for the corrosion behavior of 304 SS in Ringer's solution.

A decrease in contact angle and an increase in surface energy would lead to a better wetting of the surface by the Ringer's solution. However, there is no direct correlation between the change in contact angle and surface energy of 304 SS treated using 2, 5, and 8 mm ⌀ balls and their corrosion behavior. The corrosion resistance of treated 304 SS in Ringer's solution is not solely dependent on the contact angle and surface energy. The improvement in corrosion resistance of 304 SS treated using 2 mm ⌀ balls when compared to the untreated one is mainly attributed to the surface nanocrystallization. The nanocrystallization at the surface, refinement of grain size, selective dissolution of Fe and enrichment of Cr could provide a higher density of nucleation sites to quickly form a continuous and protective passive oxide film on 304 SS treated using 2 mm ⌀ balls when compared to the untreated one in Ringer's solution. These factors outweigh the negative influences caused by the decrease in contact angle. The increase in surface roughness, transformation of austenite to α'-martensite phase, higher extent of deformation, and presence of larger number of defects/dislocations are main factors responsible for the lower corrosion resistance of 304 SS treated using 5 and 8 mm ⌀ balls when compared to the untreated one in Ringer's solution.

Transformation of austenite to martensite phase during plastic deformation is likely to cause a deleterious influence on the corrosion resistance of 304 SS in chloride containing media.[52−55] It has been reported that the martensite phase could be selectively dissolved at potentials closer to E_{corr}, while at higher anodic potentials where the conditions are aggressive, dissolution of both austenite and martensite phases would occur.[55] Hence, transformation of austenite to martensite phase could be responsible for the more negative E_{corr} and a higher i_{corr} observed for 304 SS treated using 5 and 8 mm ⌀ balls for 15, 30, 45, and 60 min, while the absence of passive film in these samples is due to the dissolution of both phases at higher anodic potentials. In contrast, 304 SS samples treated using 2 mm ⌀ balls for 15, 30, 45, and 60 min enable a more positive E_{corr} and a slightly lower i_{corr} when compared to the untreated one, in spite of the presence of a considerable amount of martensite phase. Moreover, they exhibit good passivation characteristics. The volume fraction of α'-martensite phase is similar for samples treated using 5 and 8 mm ⌀ balls for 45 min (Figure 5). Yet, the corrosion resistance of these samples varies greatly (Figures 10 and 14 and Tables 1 and 2). These inferences point out the lack of a direct correlation between the volume fraction of the α'-martensite phase and the corrosion behavior of 304 SS subjected to SMAT. Ravi Kumar et al.[53] have also reported the absence of a direct correlation between the pitting potentials and the volume fraction of α'-martensite phase when 304L SS is subjected to cold deformation from 0 to 90%. Barbucci et al.[52] have reported that the plasticity of the material could modulate the internal stresses and hence the reactivity of the material does not solely depend on the absolute amount of martensite phase. The deleterious influence of martensite phase on the corrosion resistance of 304 SS could be clearly understood from the more negative E_{corr} and a higher i_{corr} observed for 304 SS treated using 5 and 8 mm ⌀ balls. Hence, the improved corrosion behavior of 304 SS treated using 2 mm ⌀ balls could be due to the ability of the nanocrystalline surface that promotes the dissolution of Fe in the active region and enrichment of Cr, which has resulted in the formation of an intact passive film at higher anodic potential, surpassing the deleterious influence of the martensite phase. Hence, it is clear that the corrosion resistance of 304 SS subjected to SMAT in Ringer's solution is not totally dependent on the volume fraction of α'-martensite phase and suggests that other factors such as residual stress, defects/dislocation, extent of deformation, and surface energy should also be considered in tandem.

Plastic deformation imparts stresses, strains, and defects, which could cause varied impact on the corrosion rate of materials. Fundamentally, the type and extent of residual stress would alter the free energy state of materials and their corrosion behavior. The effect of surface stress can be different depending on alloy type, treatment conditions, and environment. SMAT of 304 SS induces compressive residual stress.

DOI: 10.1021/acsami.5b03877
ACS Appl. Mater. Interfaces 2015, 7, 17731−17747

Takakuwa and Soyama[56] have reported that the critical current density for passivation and the passive current density are decreased rapidly with increasing compressive stresses in austenitic SS. According to them, the compressive residual stress induced by the cavitation jet treatment at the back side of the sample decreases the interatomic spacing and facilitates quicker passivation regardless of the surface condition. In the present study, in spite of the compressive residual stress induced by SMAT, a decrease in corrosion resistance is observed for 304 SS treated using 5 and 8 mm ⌀ balls in Ringer's solution. Hence, it is clear that the corrosion resistance of 304 SS subjected to SMAT cannot be accounted only in terms of compressive residual stress and other factors such as extent of deformation, defect density, microstrain, and surface free energy induced during SMAT should also be considered.

The extent of deformation and defect/dislocation density also play a critical role in determining the corrosion resistance of materials subjected to plastic deformation.[57,58] Cold working of nitrogen-bearing 316L SS up to 20% enhanced its pitting corrosion resistance, whereas a further increase in the extent of cold working to 30 and 40% led to a decrease in the pitting corrosion resistance.[57] Similarly, cold deformation of niobium-bearing SS up to 23% showed an improvement in corrosion resistance while an increase in the extent of deformation to 40% and 50% lead to a reversal in trend.[58] In the present study, the extent of deformation of 304 SS increased with an increase in the size of the balls and treatment time. Hence, the inferior corrosion resistance exhibited by 304 SS treated using 5 and 8 mm ⌀ balls could be due to the higher extent of deformation beyond the threshold level that could be tolerated to provide any beneficial influence on corrosion behavior.

It has been demonstrated that defects/dislocations created during deformation decreased the electron work function and reduced the energy barrier for electrochemical reactions.[59] Increase in defect/dislocation density following deformation would provide a large number of active sites and promote the rate of corrosion.[59] Increase in defect/dislocation density after SMAT has been shown to deleteriously influence the corrosion resistance.[21,22] In the present study, the CTT shows a higher current density for 304 SS treated using 5 and 8 mm ⌀ balls (Figure 11), which can be correlated to the presence of higher amounts defects/dislocations in them than in those treated using 2 mm ⌀ balls and the untreated one. According to Inturi and Szklarska-Smialowska,[60] the presence of a large number of defects in nanocrystalline materials enables a high degree of distribution of chloride ions on the surface. Hence, localized enrichment of chloride ions and subsequent acidification at each defect site on the grain boundary requires a greater driving force for the occurrence of localized corrosion attack. The surface morphology of the samples after CTT clearly reveals that the extent of localized attack is relatively less for 304 SS treated using 5 and 8 mm ⌀ 316L SS balls (marked with squares in Figure 12e,f). The higher amounts of defects/dislocation density could have enabled a high degree of distribution of Cl^- ions on the surface, which promotes general corrosion, following acidification of the entire surface, rather than the localized corrosion attack. The extent of corrosion attack becomes severe (general corrosion) and delamination of the deformed region (marked with arrows in Figure 12e,f) confirms penetration of the electrolyte through the surface defects created during SMAT. In contrast, the surface morphology of 304 SS treated using 2 mm ⌀ balls for 15 and 30 min has not suffered much with severe corrosion attack, while those treated using 2 mm ⌀ balls for 60 min exhibits a larger pit growth (marked with a square in Figure 12d).

On the basis of the inferences made in the present study, it is clear that the increase in surface roughness, transformation of the austenite to martensite phase, higher extent of deformation, and presence of larger number of defects/dislocations are main factors responsible for the lower corrosion resistance observed for 304 SS treated using 5 and 8 mm ⌀ balls in Ringer's solution. In spite of having these attributes with a relatively lower extent, 304 SS treated using 2 mm ⌀ balls offers a better corrosion resistance and exhibits a better passivity. This is primarily due to the ability of the nanocrystalline surface that promotes passivation, thus outweighing any deleterious influences caused by the limited amount of deformation and defects/dislocations. For 304 SS treated using 5 and 8 mm ⌀ balls, the beneficial influence of the nanocrystalline surface could not be realized, and it is compensated by the negative influence of higher extent of deformation, higher volume fraction of martensite phase, and larger number of defects/dislocations. The deleterious influence of the martensite phase is also reflected in 304 SS treated using 2 mm ⌀ balls, resulting in a lower E_b in spite of their more positive E_{corr} and lower i_{corr}. Hence, it is evident that surface nanostructuring is beneficial in terms of promoting passivation and improving the corrosion resistance of 304 SS in Ringer's solution. Nevertheless, optimizing the processing conditions is very critical to achieve the same. For the experimental conditions used in the present study, SMAT of 304 SS using 2 mm ⌀ 316L SS balls at 50 Hz for a period of up to 15−30 min appears to be optimal in terms of surface characteristics and corrosion resistance in Ringer's solution.

5. CONCLUSION

SMAT of 304 SS induced plastic deformation, enabled nanocrystallization at the surface, and refined the grain size. The extent of deformation at the surface of 304 SS is increased with an increase in treatment time and size of the balls. The multidirectional impingement of the SS balls increased the surface roughness, decreased the contact angle and increased the surface energy of the treated surface. The plastic deformation of the surface also lead to transformation of the austenite to strain induced α'-martensite phase, induced defects/dislocations and imparted compressive residual stresses. The change in surface properties leads to a significant change in the corrosion behavior of treated 304 SS. The increase in surface roughness, transformation of the austenite to α'-martensite phase, higher extent of deformation, and presence of larger number of defects/dislocations are main factors responsible for the lower corrosion resistance of 304 SS treated using 5 and 8 mm ⌀ balls when compared to the untreated one in Ringer's solution. The nanocrystallization at the surface, refinement of grain size, selective dissolution of Fe and enrichment of Cr could provide a higher density of nucleation sites to quickly form a continuous and protective passive oxide film on 304 SS treated using 2 mm ⌀ balls when compared to the untreated one in Ringer's solution. Surface nanostructuring of 304 SS by SMAT is beneficial in terms of promoting passivation, increasing the hardness and mechanical properties, decreasing the contact angle, and increasing the wettability. Nevertheless, to achieve an improvement in corrosion resistance in Ringer's solution, the extent of deformation, defects/dislocations induced during treatment, and the increase in surface roughness should be limited to a certain extent,

DOI: 10.1021/acsami.5b03877
ACS Appl. Mater. Interfaces 2015, 7, 17731−17747

beyond which a deleterious influence on corrosion resistance is observed. The corrosion behavior of treated 304 SS in Ringer's solution is not solely determined by grain refinement while other factors such as increase surface roughness, transformation of austenite to strain induced α'-martensite phase, defects/dislocations and residual stresses induced during SMAT, also play a major role. Establishing a direct correlation of the corrosion behavior of treated 304 SS with any one of these factors is difficult and complex because it is influenced by more than one factor at a time. All these factors, either individually or in combination, could influence the corrosion resistance of the treated 304 SS. For the experimental conditions used in the present study, SMAT of 304 SS using 2 mm ⌀ 316L SS balls at 50 Hz for a period of up to 15−30 min appears to be optimal in terms of improved surface characteristics and corrosion resistance in Ringer's solution.

■ ASSOCIATED CONTENT

Supporting Information

The Supporting Information is available free of charge on the ACS Publications website at DOI: 10.1021/acsami.5b03877.

Non-linear least square fitting, Bode impedance, and phase angle plots (PDF)

■ AUTHOR INFORMATION

Corresponding Authors

*E-mail: tsnsn@rediffmail.com.
*E-mail: mh@jbnu.ac.kr.

Notes

The authors declare no competing financial interest.

■ ACKNOWLEDGMENTS

T.B. and T.S.N. Sankara Narayanan express their sincere thanks to Dr. S. Srikanth, Director, CSIR-National Metallurgical Laboratory, Jamshedpur, for his constant support and encouragement to carry out this research work and permission to publish this paper. This work was also financially supported by the National Research Foundation of Korea (NRF) grant funded by the Korea government (MSIP) (2011-0028709, 2013R1A1A2012322 and 2014R1A4A1005309) and Regional Strategic Industry project (2013-R0002274). This work was also supported by the research funds of Chonbuk National University in 2013 and 2014.

■ REFERENCES

(1) Lee, W.; Park, S.-J. Porous Anodic Aluminum Oxide: Anodization and Templated Synthesis of Functional Nanostructures. *Chem. Rev.* **2014**, *114* (15), 7487−7556.

(2) Liu, Y.; Goebl, J.; Yin, Y. Templated Synthesis of Nanostructured Materials. *Chem. Soc. Rev.* **2013**, *42*, 2610−2653.

(3) Valiev, R. Z.; Sabirov, I.; Zhilyaev, A. P.; Langdon, T. G. Bulk Nanostructured Metals for Innovative Applications. *JOM* **2012**, *64*, 1134−1142.

(4) Bagherifard, S.; Ghelichi, R.; Khademhosseini, A.; Guagliano, M. Cell Response to Nanocrystallized Metallic Substrates Obtained through Severe Plastic Deformation. *ACS Appl. Mater. Interfaces* **2014**, *6*, 7963−7985.

(5) Lu, K.; Lu, J. Surface Nanocrystallization (SNC) of Metallic Materials-Presentation of the Concept Behind a New Approach. *J. Mater. Sci. Technol.* **1999**, *15*, 193−197.

(6) Bahl, S.; Shreyas, P.; Trishul, M. A.; Suwas, S.; Chatterjee, K. Enhancing the Mechanical and Biological Performance of a Metallic Biomaterial for Orthopedic Applications through Changes in the Surface Oxide Layer by Nanocrystalline Surface Modification. *Nanoscale* **2015**, *7*, 7704−7716.

(7) Huang, H. W.; Wang, Z. B.; Lu, J.; Lu, K. Fatigue Behaviors of AISI 316L Stainless Steel with a Gradient Nanostructured Surface Layer. *Acta Mater.* **2015**, *87*, 150−160.

(8) Balusamy, T.; Sankara Narayanan, T. S. N.; Ravichandran, K.; Park, I. S.; Lee, M. H. Surface Mechanical Attrition Treatment (SMAT) on Pack Boronizing of AISI 304 Stainless Steel. *Surf. Coat. Technol.* **2013**, *232*, 60−67.

(9) Balusamy, T.; Sankara Narayanan, T. S. N.; Ravichandran, K.; Park, I. S.; Lee, M. H. Plasma Nitriding of AISI 304 Stainless Steel: Role of Surface Mechanical Attrition Treatment. *Mater. Charact.* **2013**, *85*, 38−47.

(10) Chandrasekaran, K.; Nellaiappan, S. N. T. S.; Kulandaivelu, R.; Lee, M. H. Improving the Reactivity and Receptivity of Alloy and Tool Steels for Phosphate Conversion Coatings: Role of Surface Mechanical Attrition Treatment. *Ind. Eng. Chem. Res.* **2014**, *53*, 20124−20138.

(11) Zhao, C.; Han, P.; Ji, W.; Zhang, X. Enhanced Mechanical Properties and in Vitro Cell Response of Surface Mechanical Attrition Treated Pure Titanium. *J. Biomater. Appl.* **2012**, *27*, 113−118.

(12) Estrin, Y.; Ivanova, E. P.; Michalska, A.; Truong, V. K.; Lapovok, R.; Boyd, R. Accelerated Stem Cell Attachment to Ultra-fine grained Titanium. *Acta Biomater.* **2011**, *7*, 900−906.

(13) Lai, M.; Cai, K.; Hu, Y.; Yang, X.; Liu, Q. Regulation of the Behaviors of Mesenchymal Stem Cells by Surface Nanostructured Titanium. *Colloids Surf., B* **2012**, *97*, 211−220.

(14) Huang, R.; Lu, S.; Han, Y. Role of Grain Size in the Regulation of Osteoblast Response to Ti−25Nb−3Mo−3Zr−2Sn alloy. *Colloids Surf., B* **2013**, *111*, 232−241.

(15) Gittens, R. A.; McLachlan, T.; Olivares-Navarrete, R.; Cai, Y.; Berner, S.; Tannenbaum, R.; Schwartz, Z.; Sandhage, K. H.; Boyan, B. D. The Effects of Combined Micron-/Submicron-Scale Surface Roughness and Nanoscale Features on Cell Proliferation and Differentiation. *Biomaterials* **2011**, *32*, 3395−3403.

(16) Misra, R. D. K.; Nune, C.; Pesacreta, T. C.; Somani, M. C.; Karjalainen, L. P. Understanding the Impact of Grain Structure in Austenitic Stainless Steel from a Nanograined Regime to a Coarse-Grained Regime on Osteoblast Functions Using a Novel Metal Deformation−Annealing Sequence. *Acta Biomater.* **2013**, *9*, 6245−6258.

(17) Roland, T.; Retraint, D.; Lu, K.; Lu, J. Fatigue Life Improvement Through Surface Nanostructuring of Stainless Steel by Means of Surface Mechanical Attrition Treatment. *Scr. Mater.* **2006**, *54*, 1949−1954.

(18) Sun, Y.; Bailey, R. Improvement in Tribocorrosion Behavior of 304 Stainless Steel by Surface Mechanical Attrition Treatment. *Surf. Coat. Technol.* **2014**, *253*, 284−291.

(19) Ralston, K. D.; Birbilis, N.; Davies, C. H. J. Revealing the Relationship between Grain Size and Corrosion Rate of Metals. *Scr. Mater.* **2010**, *63*, 1201−1204.

(20) Gupta, R. K.; Birbilis, N. The Influence of Nanocrystalline Structure and Processing Route on Corrosion of Stainless Steel: A review. *Corros. Sci.* **2015**, *92*, 1−15.

(21) Balusamy, T.; Kumar, S.; Sankara Narayanan, T. S. N. Effect of Surface Nanocrystallization on the Corrosion behavior of AISI 409 Stainless Steel. *Corros. Sci.* **2010**, *52*, 3826−3834.

(22) Balusamy, T.; Sankara Narayanan, T. S. N.; Ravichandran, K.; Lee, M. H.; Nishimura, T. Surface Nanocrystallization of EN8 Steel: Correlation of Change in Material Characteristics with Corrosion Behavior. *J. Electrochem. Soc.* **2015**, *162*, C285−C293.

(23) Samih, Y.; Beausir, B.; Bolle, B.; Grosdidier, T. In-depth Quantitative Analysis of the Microstructures Produced by Surface Mechanical Attrition Treatment (SMAT). *Mater. Charact.* **2013**, *83*, 129−138.

(24) Tsai, W. Y.; Huang, J. C.; Gao, Y. J.; Chung, Y. L.; Huang, G. R. Relationship between Microstructure and Properties for Ultrasonic Surface Mechanical Attrition Treatment. *Scr. Mater.* **2015**, *103*, 45−48.

DOI: 10.1021/acsami.5b03877
ACS Appl. Mater. Interfaces 2015, 7, 17731−17747

(25) Nowell, M. M.; Witt, R. A.; True, B. W. EBSD Sample Preparation: Techniques, Tips, and Tricks. *Microsc. Microanal.* **2005**, *11*, 44−48.
(26) Vives, S.; Gaffet, E.; Meunier, C. X-ray Diffraction Line Profile Analysis of Iron Ball Milled Powders. *Mater. Sci. Eng., A* **2004**, *366*, 229−238.
(27) Lee, H. S.; Kim, D. S.; Jung, J. S.; Pyoun, Y. S.; Shin, K. Influence of Peening on the Corrosion Properties of AISI 304 Stainless Steel. *Corros. Sci.* **2009**, *51*, 2826−2830.
(28) Franxois, M.; Sprauel, J. M.; Dehan, C. F.; James, M. R.; Convert, F.; Lu, J. X-Ray Diffraction Method. In *Handbook of Measurement of Residual Stresses*; Lu, J., Ed.; Fairmont Press, Society for Experimental Mechanics: Lilburn, GA, 1996; pp 71−133.
(29) Huang, C. C.; Pan, Y. C.; Chuang, T. H. Effects of Post-Weld Heat Treatments on the Residual Stress and Mechanical Properties of Electron Beam Welded SAE 4130 Steel Plates. *J. Mater. Eng. Perform.* **1997**, *6*, 61−68.
(30) Khang, D.; Lu, J.; Yao, C.; Haberstroh, K. M.; Webster, T. J. The Role of Nanometer and Sub-micron Surface Features on Vascular and Bone Cell Adhesion on Titanium. *Biomaterials* **2008**, *29*, 970−983.
(31) Liu, X.; Lim, J. Y.; Donahue, H. J.; Dhurjati, R.; Mastro, A. M.; Vogler, E. A. Influence of Substratum Surface Chemistry/Energy and Topography on the Human Fetal Osteoblastic Cell Line hFOB 1.19: Phenotypic and Genotypic Responses Observed in vitro. *Biomaterials* **2007**, *28* (31), 4535−4550.
(32) Hedayati, A.; Najafizadeh, A.; Kermanpur, A.; Forouzan, F. The Effect of Cold Rolling Regime on Microstructure and Mechanical Properties of AISI 304L Stainless Steel. *J. Mater. Process. Technol.* **2010**, *210*, 1017−1022.
(33) Zhang, H. W.; Hei, Z. K.; Liu, G.; Lu, J.; Lu, K. Formation of Nanostructured Surface Layer on AISI 304 Stainless Steel by means of Surface Mechanical Attrition Treatment. *Acta Mater.* **2003**, *51*, 1871−1881.
(34) Liu, S.; Gao, S. Y.; Zhou, Y. F.; Xing, X. L.; Hou, X. R.; Yang, Y. L.; Yang, Q. X. A Research on The Microstructure Evolution of Austenite Stainless Steel by Surface Mechanical Attrition Treatment. *Mater. Sci. Eng., A* **2014**, *617*, 127−138.
(35) Ye, C.; Telang, A.; Gill, A. S.; Suslov, S.; Idell, Y.; Zweiacker, K.; Wiezorek, J. M. K.; Zhou, Z.; Qian, D.; Mannava, S. R.; Vasudevan, V. K. Gradient Nanostructure and Residual Stresses Induced by Ultrasonic Nano-crystal Surface Modification in 304 Austenitic Stainless Steel for High Strength and High Ductility. *Mater. Sci. Eng., A* **2014**, *613*, 274−288.
(36) Shen, Y. F.; Li, X. X.; Sun, X.; Wang, Y. D.; Zuo, L. Twinning and Martensite in a 304 Austenitic Stainless Steel. *Mater. Sci. Eng., A* **2012**, *552*, 514−522.
(37) Arifvianto, B.; Suyitno; Mahardika, M.; Dewo, P.; Iswanto, P. T.; Salim, U. A. Effect of Surface Mechanical Attrition Treatment (SMAT) on Microhardness, Surface Roughness and Wettability of AISI 316L. *Mater. Chem. Phys.* **2011**, *125*, 418−426.
(38) Anand Kumar, S.; Ganesh Sundara Raman, S.; Sankara Narayanan, T. S. N.; Gnanamoorthy, R. Fretting Wear Behaviour of Surface Mechanical Attrition Treated alloy 718. *Surf. Coat. Technol.* **2012**, *206*, 4425−4432.
(39) Mordyuk, B. N.; Prokopenko, G. I. Ultrasonic Impact Peening for the Surface Properties' Management. *J. Sound Vibration* **2007**, *308*, 855−866.
(40) Chen, T.; John, H.; Xu, J.; Lu, Q.; Hawk, J.; Liu, X. Influence of Surface Modifications on Pitting Corrosion Behavior of Nickel-base Alloy 718. Part 1: Effect of Machine Hammer Peening. *Corros. Sci.* **2013**, *77*, 230−245.
(41) Li, N.; Li, Y. D.; Li, Y. X.; Wu, Y. H.; Zheng, Y. F.; Han, Y. Effect of Surface Mechanical Attrition Treatment on Biodegradable Mg−1Ca Alloy. *Mater. Sci. Eng., C* **2014**, *35*, 314−321.
(42) Jamesh, M.; Sankara Narayanan, T. S. N.; Chu, P. K.; Park, I. S.; Lee, M. H. Effect of Surface Mechanical Attrition Treatment of Titanium Using Alumina Balls: Surface Roughness, Contact Angle and Apatite Forming Ability. *Front. Mater. Sci.* **2013**, *7*, 285−294.
(43) Chui, P.; Sun, K.; Sun, C.; Yang, X.; Shan, T. Effect of Surface Nanocrystallization Induced by Fast Multiple Rotation Rolling on Hardness and Corrosion Behavior of 316L Stainless Steel. *Appl. Surf. Sci.* **2011**, *257*, 6787−6791.
(44) Azar, V.; Hashemi, B.; Yazdi, M. R. The Effect of Shot Peening on Fatigue and Corrosion Behavior of 316L Stainless Steel in Ringer's Solution. *Surf. Coat. Technol.* **2010**, *204*, 3546−3551.
(45) Ralston, K. D.; Birbilis, N. Effect of Grain Size on Corrosion: A Review. *Corrosion* **2010**, *66*, 075005−075005−13.
(46) Pan, C.; Liu, L.; Li, Y.; Wang, S.; Wang, F. Passive Film Growth Mechanism of Nanocrystalline 304 Stainless Steel Prepared by Magnetron Sputtering and Deep Rolling Techniques. *Electrochim. Acta* **2011**, *56*, 7740−7748.
(47) Wang, T.; Yu, J.; Dong, B. Surface Nanocrystallization Induced by Shot Peening and its Effect on Corrosion resistance of 1Cr18Ni9Ti Stainless Steel. *Surf. Coat. Technol.* **2006**, *200*, 4777−4781.
(48) Maleki-Ghaleh, H.; Hajizadeh, K.; Aghaie, E.; Ghobadi Alamdari, S.; Hosseini, M. G.; Fathi, M. H.; Ozaltin, K.; Kurzydlowski, K. J. Effect of Equal Channel Angular Pressing Process on the Corrosion Behavior of Type 316L Stainless Steel in Ringer's Solution. *Corrosion* **2015**, *71*, 367−375.
(49) Jindal, S.; Bansal, R.; Singh, B. P.; Pandey, R.; Sankara Narayanan, T. S. N.; Wani, M. R.; Singh, V. Enhanced Osteoblast Proliferation and Corrosion Resistance of Commercially Pure Titanium Through Surface Nanostructuring by Ultrasonic Shot Peening and Stress Relieving. *J. Oral Implantology* **2014**, *40*, 347−355.
(50) Shahryari, A.; Kamal, W.; Omanovic, S. The Effect of Surface Roughness on the Efficiency of the Cyclic Potentiodynamic Passivation (CPP) Method in the Improvement of General and Pitting Corrosion Resistance of 316LVM Stainless Steel. *Mater. Lett.* **2008**, *62*, 3906−3909.
(51) Lee, S. M.; Lee, W. G.; Kim, Y. H.; Jang, H. Surface Roughness and the Corrosion Resistance of 21Cr Ferritic Stainless Steel. *Corros. Sci.* **2012**, *63*, 404−409.
(52) Barbucci, A.; Cerisola, G.; Cabot, P. L. Effect of Cold- Working in the Passive Behavior of 304 Stainless Steel in Sulfate Media. *J. Electrochem. Soc.* **2002**, *149*, B534−B542.
(53) Ravi Kumar, B.; Mahato, B.; Singh, R. Influence of Cold-Worked Structure on Electrochemical Properties of Austenitic Stainless Steels. *Metall. Mater. Trans. A* **2007**, *38*, 2085−2094.
(54) Peguet, L.; Malki, B.; Baroux, B. Effect of Austenite Stability on the Pitting Corrosion Resistance of Cold Worked Stainless Steels. *Corros. Sci.* **2009**, *51*, 493−498.
(55) Alvarez, S. M.; Bautista, A.; Velasco, F. Influence of Strain-induced Martensite in the Anodic dissolution of Austenitic Stainless Steels in Acid Medium. *Corros. Sci.* **2013**, *69*, 130−138.
(56) Takakuwa, O.; Soyama, H. Effect of Residual Stress on the Corrosion Behavior of Austenitic Stainless Steel. *Adv. Chem. Eng. Sci.* **2015**, *5*, 62−71.
(57) Kamachi Mudali, U.; Shankar, P.; Ningshen, S.; Dayal, R. K.; Khatak, H. S.; Raj, B. On the Pitting Corrosion Resistance of Nitrogen Alloyed Cold Worked Austenitic Stainless Steels. *Corros. Sci.* **2002**, *44*, 2183−2198.
(58) Hamdy, A. S.; El-Shenaw, E.; El-Bitar, T. Electrochemical Impedance Spectroscopy Study of the Corrosion Behavior of Some Niobium Bearing Stainless Steels in 3.5% NaCl. *Int. J. Electrochem. Sci.* **2006**, *1*, 171−180.
(59) Li, W.; Li, D. Y. Variations of Work Function and Corrosion Behaviors of Deformed Copper Surfaces. *Appl. Surf. Sci.* **2005**, *240*, 388−395.
(60) Inturi, R. B.; Szklarska-Smialowska, Z. Localized Corrosion of Nanocrystalline 304 Type Stainless Steel Films. *Corrosion* **1992**, *48*, 398−403.

DOI: 10.1021/acsami.5b03877
ACS Appl. Mater. Interfaces 2015, 7, 17731−17747